Establishment of Tricultures in Microfluidic Platforms

Miguel Guilherme Linhas Simões

Integrated Masters in Bioengineering – Molecular Biotechnology

Supervisor: Dr Meriem Lamghari (i3S)
Co-supervisor: Dr Estrela Neto (i3S)

Porto, September 2018

The work described in this thesis was conducted at:

i3S/INEB - Instituto de Investigação e Inovação em Saúde; Universidade do Porto

The work described in this thesis was financially supported by:

This work was financed by FEDER - Fundo Europeu de Desenvolvimento Regional funds through the COMPETE 2020 - Operacional Programme for Competitiveness and Internationalisation (POCI), Portugal 2020, and by Portuguese funds through FCT/MCTES in the framework of the project "Institute for Research and Innovation in Health Sciences" (POCI-01-0145-FEDER-007274) and the project PTDC/BIM-MED/4041/2014.

This page was intentionally left in blank

Acknowledgements

Firstly, I would like to thank Estrela for all the support, guidance, patience, and availability throughout the period I was under her supervision. Not only have I learned important laboratory skills, but also how to be patient and perseverant when facing difficult situations.

Secondly, I want to express my gratitude to Professor Meriem Lamghari for the opportunity to be a part of her research team and learn about several subjects I was mostly new to, but most importantly, for the guidance and insight during these studies. On this note, I also would like to thank to Professor Maria José Oliveira for helping me getting in contact with Professor Meriem.

I am also thankful to all members of the Nesk team for all the help provided during this work, specially to Luís, for all the support during the final stages of this dissertation, and the fun football matches every Monday. I have felt welcomed and supported since day one, whether in or outside the laboratory. Similarly, the nBTT members have all contributed to a pleasant and motivating work environment, helping with suggestions and answers to all details, particularly the soon to be PhD students. I am also grateful for the support of the lab technicians, namely Dalila and Ricardo, who were fundamental for the experiments here presented. Moreover, I want to express my gratitude towards the Biointerfaces and Nanotechnology Core Facility and Advanced Light Microscopy group, specially María, Paula Sampaio and Maria, for the teachings and help using the equipment necessary for this work.

I want to thank to my friends, and to those who shared the hardships of this master thesis with me, specially Sofia, for her insight, calmness, laughs and coffees shared together.

Lastly, I want to thank my parents and brother for the patience and invaluable support, especially during the final stages of this road.

This page was intentionally left in blank

Abstract

Bone homeostasis is a result of concerted interactions between bone cells and their surrounding microenvironment. Vascularization and innervation have been implied as fundamental players in bone development, homeostasis, and regeneration, and are often coupled both anatomically and physiologically. Although it is known that osteoclasts interact with endothelial cells and respond to neuropeptides released by nerve fibers, the interaction mechanisms between osteoclastogenesis, innervation and vascularization remain to be fully understood. Moreover, current *in vitro* models lack the complexity required to study these cross talks, since bone vascularized models do not usually include innervation and vice-versa.

In this project, a triculture composed of sensory neurons, endothelial cells, and osteoclasts was assembled within a microfluidic device, given the possibility of culturing different cell types under precisely controlled conditions. This goal was achieved through a step-by-step process. In addition, the angiogenic potential of osteoclasts was assessed through a tube formation assay.

The first part of the project consisted in optimizing the 3D culture of human umbilical vein endothelial cells within different hydrogels with angiogenic potential: Matrigel®, fibrin and collagen/fibrin mixture. Different cell densities were tested, from which $20x10^6$ cells/mL proved to be the most suitable for the formation of vascular networks. In addition, throughout the 96 hours culture period, cells were shown to remain viable and metabolically active. Consequently, the collagen/fibrin hydrogels and Matrigel® were chosen to support human umbilical vein endothelial cell culture within the microfluidic platforms. After 72 hours it was observed the formation of vascular networks and CD31 expression. Interestingly, cells were found to coat the microchannels forming a lumen-like structure.

The next step consisted of co-culturing sensory neurons and endothelial cells, seeded in Matrigel®, in separate compartments. Axonal outgrowth occurred from the neuronal compartment towards the endothelial cells, possibly indicating a supportive effect of the endothelial cells on the nerve growth.

The triculture of sensory neurons, endothelial cells, and human osteoclasts was performed using Matrigel® or collagen/fibrin hydrogels. Technical difficulties during the seeding of endothelial cells compromised the proper separation between compartments. No neurite projections have reached the endothelial cells

compartment, possibly due to impaired culture viability. As a result, further optimization is required.

Lastly, the angiogenic potential of osteoclasts was assessed through a tube formation assay. Even though no tube formation was observed, preliminary observations have shown that osteoclast conditioned medium may promote endothelial cell survivability, but further optimization is required.

To conclude, during this dissertation, endothelial cell culture was optimized to be included in a vascularized bone mimicking triculture model comprised of sensory neurons, endothelial cells, and human osteoclasts. The angiogenic potential of osteoclasts was also assessed. However, both these experiments require further optimization to conclude about the biological interactions between these cells.

Table of contents

List of figures

Abbreviations and Symbols

2D	Two Dimensional
3D	Three Dimensional
Agc	Aggrecan
ALP	Alkaline Phosphatase
Ang-1	Angiopoietin-1
Atp6v0d2	D2 isoform of vacuolar (H+) ATPase (v-ATPase) V0 domain
BMA-EDMA	butyl methacrylate-ethylene dimethacrylate
BM-hMSC	Human Bone Marrow-derived Mesenchymal Stem Cell
BMP	Bone Morphogenic Proteins
BMU	Basic Multicellular Unit
BS	Bone Slices
CC3a	Complement Component 3a
CGRP	Calcitonin-Gene Related Peptide
CM	Conditioned Medium
CNS	Central Nervous System
Col/Fib	Collagen/Fibrin
Col2a1	Collagen II
DRG	Dorsal Root Ganglion
ECGS	Endothelial Cell Growth Supplement
ECM	Extra Cellular Matrix
ECs	Endothelial Cells
EGFR	Epidermal Growth Factor Receptor
EGM-2	Endothelial Cell Growth Medium-2
Emcn1	Endomucin
EPC	Endothelial Progenitor Cell
ErbB2	Erythroblastic Leukemia Viral Oncogene Homolog 2
FBS	Fetal bovine serum
HA	Hydroxyapatite
HMVEC	Human Microvascular Endothelial Cell
hOC CM	Human Osteoclast Conditioned Medium
hOC	human Osteoclast
HUVEC	Human Umbilical Vein Endothelial Cell

HVEC	Human Vascular Endothelial Cells
MAPK	Mitogen-Activated Protein Kinase Pathways
MCSF	Macrophage Colony Stimulating Factor
mL	Milliliter
MMP-9	matrix metalloprotein-9
MSC	Mesenchymal Stem Cells
Ntn4	Netrin4
OCN	Osteocalcin
OPG	Osteoprotegrin
Osterix	OSX
P/S	Penicillin/Streptomycin
PBMC	Peripheral Blood Mononuclear Cells
PDGF-BB	Platelet-derived growth factor BB
PDL	Poly-D-lysine
PDMS	Polydimethylsiloxane
PFA	Paraformaldehyde
PKA	Protein Kinase A
POC	Primary ossification center
RAMPs	Receptor Activity Modifying Proteins
RANKL	Receptor Activator of NF-κB ligand
RBC	Red Blood Cells
Sema-4D	Semaphorin-4D
SP	Substance P
TCPS	Tissue Culture Polystyrene
TGF-β	Transforming Growth Factor β
TNF	Tumor Necrosis Factor
TRAcP	Tartare Resistant Acid Phosphatase
TRAF6	TNF receptor associated factor 6
TRIP-1	Receptor-Interacting Protein
VEC	Vascular Endothelial Cells
vWF	von Willebrand factor
α-SMA	Alpha-smooth Muscle Actin
β-NGF	β-nerve growth factor

Chapter I: Literature Review

Bone structure

Bone is a dense, dynamic, mineralized connective tissue that takes part in multiple important physiological functions within our body, such as locomotion, mechanical support and load bearing, protection of soft tissues, storage of calcium and phosphate ions and is the site of storage and production of bone marrow [1,2.] Macroscopically, bone tissue (Figure 1) is categorized as cortical or compact bone (about 80% of the total skeleton), and trabecular, also indicated as cancellous or spongy bone (about 20% of the total skeleton). The former, located mostly in the diaphysis of long bones, comprises dense and compact tissue pierced by blood vessels and canaliculi surrounding osteocytes and their connecting cellular processes; compact bone can also be divided into different categories: long bones, short bones and flat bones. The latter, trabecular bone, is commonly present in metaphysis of long bones, vertebrae and close to joint surfaces. It consists of trabeculae: plates, bars and rods of different sizes arranged in a honeycomb manner, surrounded by bone marrow. Its structure grants trabecular bone increased porosity (ranging between 50% and 90%, as opposed to cortical bone's 10%). Although similar in molecular and cellular content, the different structural arrangement between cortical and trabecular bone translates into distinct functional and mechanical properties[1-3]. On the one hand, cortical bone, thanks to its dense structure, grants resistance to torsion and bending. On the other hand, cancellous bone assures mechanical flexibility[4].

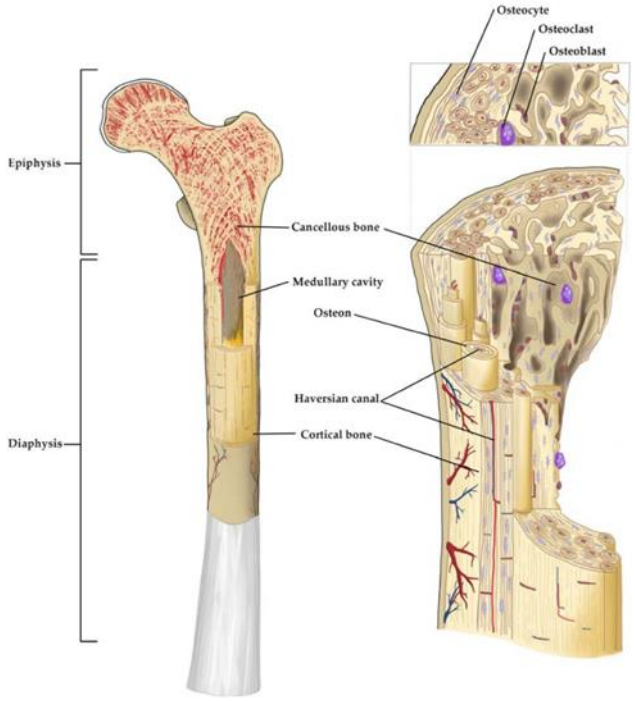

Figure 1-Bone anatomical elements and cell populations. Adapted from Scheinpflug, Pfeiffenberger et al.[4]

1. Matrix and Cellular elements

Bone homeostasis is achieved through the coordination between the different cell populations, in a process called bone remodeling. Within the bone, three major cell types can be found: the osteoblasts, responsible for producing bone matrix; the tissue-resorbing osteoclast; and the osteocyte, which represents the highest percentage of cells in the bone. The extra cellular matrix (ECM) that supports bone cells is comprised of organic matrix, inorganic elements, lipids and water. The organic matrix accounts for 30% of the ECM, mainly consists of collagen I and is responsible for providing elasticity and flexibility. On the other hand, the inorganic elements constitute 60% of the ECM, being responsible for its mechanical stability. This mineralized part of the bone has as its main component hydroxyapatite (HA) crystals, formed by calcium and phosphorus. Contrary to the organic fraction, the HA crystals give bone mechanical rigidity and load-bearing capacities[4].

1.1. Osteocytes

The osteocytes are former osteoblasts that became entrapped within the bone matrix during the bone deposition process. These are star-shaped cells that communicate through canaliculi, gap junctions and dendritic processes. Osteocytes present similar gene expression profiles to osteoblasts, including osteoblast-specific transcription factors and proteins. However, not at similar levels. For instance, alkaline phosphatase (ALP) and collagen I expression is lower, but osteocalcin is higher. Osteocytes have an important role in the regulation of osteoblastic activity due to the expression of Wnt and bone morphogenic proteins (BMP) antagonists, for instance sclerostin, a strong inhibitor of bone formation[5]. Variations in sclerostin expression are responsible for adaptive changes of the skeleton to mechanical stimulation. Whereas cortical bone areas subject to high mechanical strain show lower numbers of sclerostin-positive osteocytes, associated with higher bone formation, unloaded bones display higher expression levels of SOST/sclerostin. These observations also identify osteocytes as regulators of bone formation through response to mechanical stimulation by downregulating sclerostin and subsequently promoting Wnt signalling. In addition, osteocytes also interfere with the resorption activity of osteoclasts, by meddling with the receptor activator of NF-κB ligand (RANKL)/ osteoprotegrin (OPG) balance. Osteocytes may indirectly stimulate osteoclastogenesis by inducing production on RANKL by stromal/osteoblastic cells, and directly by producing RANKL themselves. In contrast, osteocytes also secrete OPG that produces contrary effects to RANKL[5].

1.2. Osteoblasts

Osteoblasts are cuboid shaped cells derived from mesenchymal stem cells (MSC) located along the bone surface, mostly known for their bone formation function. The commitment towards the osteoprogenitor demands the expression of specific genes, followed by well-orchestrated events that include the synthesis of BMPs as well members of the Wnt pathways. The crucial genes expressed during osteoblastic differentiation are Runx2, Dlx5 and osterix (Osx). *Runx2* is a master regulator of osteoblast differentiation whose absence impairs osteoblast formation and is involved in the upregulation of osteoblast-related genes, such as *ColIA1*, *ALP*, *BSP*, *BGLAP*, and *OCN*. After a group of *Runx2 and ColIA1* expressing osteoblast progenitors has been set upon osteoblast differentiation, the proliferation phase takes place. During this stage, osteoblast progenitors become preosteoblasts based on their ALP activity. The transformation into mature osteoblasts is indicted by the increase in the expression of

Osx and secretion of bone matrix proteins, namely osteocalcin (OCN), bone sialoprotein (BSP) I/II and collagen type I. Simultaneously, osteoblasts suffer morphological changes, turning into larger and cuboid shaped cells[6].

The formation of new bone matrix by osteoblasts comprises two different stages: firstly, there is an accumulation of organic matrix, followed by its mineralization. The organic matrix deposited in the first stage is composed of collagen proteins, mainly type I collagen, non-collagen proteins (OCN, osteonectin, BSP II, and osteopontin), and proteoglycan including decorin and biglycan. The subsequent matrix mineralization takes place in two phases: the vesicular and fibrillar phases. In the vesicular phase, matrix vesicles are released from the apical membrane domain of the osteoblasts into the previously formed matrix, binding to proteoglycans and other organic components. During this stage, both calcium and phosphate ions are entrapped within the matrix vesicles. The calcium ions, previously bound to negatively charged sulphated proteoglycans degraded by enzymes secreted by osteoblasts, cross the matrix vesicles' membrane through calcium channels formed by annexins. The phosphate ions are originated through the breakdown of phosphate-containing compounds by the ALP. Together, the calcium and phosphate ions within the matrix vesicles form HA crystals. The fibrillar phase ensures these HA crystals are spread to the surrounding matrix once the supersaturation of calcium and phosphate ions inside the matrix vesicles leads to the rupture of these structures[2].

The osteoblasts that have surrounded themselves with newly formed bone matrix will eventually differentiate into osteocytes, whereas osteoblasts that have remained on the surface of bone facing periosteum have the option of becoming inert bone-lining cells or undergo apoptosis. Upon the decrease of mature osteoblasts, new osteoblasts are differentiated from mesenchymal progenitor cells[6,7].

1.3. Osteoclasts

The differentiation of myeloid precursors, promoted by the cytokines macrophage colony stimulating factor (MCSF) and RANKL, secreted by osteoblasts and/or osteocytes, originates multinucleated giant cells called osteoclasts. RANKL is the key player of osteoclast formation in response to all known stimuli[7]. RANKL is a 317 amino acid peptide, member of the tumor necrosis factor (TNF) superfamily, expressed by osteoblast lineage cells that interacts with the RANK receptor of osteoclast precursors. The binding between RANKL and its receptor activates the TNF receptor associated factor 6 (TRAF6), which stimulates the NF-κB and mitogen-activated protein kinase pathways (MAPK)[8]. The interaction between the RANK

receptor and its ligand is responsible for the activation, differentiation and fusion of osteoclast precursors, thereby initiating the process of resorption[9].

The main function of osteoclasts is bone resorption during bone remodeling, a process that ensures bone growth, repair and regulation of calcium and phosphate metabolism[10]. Bone resorption is possible due to osteoclasts' unique structure (Figure 2) and morphology. Particularly peculiar is its ability to polarize and segregate unique plasma membrane domains that support its local digestive extracellular function. Osteoclasts present an apical membrane facing the bone and a basolateral membrane facing the vascular stream. The apical membrane consists of different areas: the sealing zone and the ruffled border. The sealing zone itself comprises the sealing membrane, an outer circular domain equipped with adhesion structures called podosomes, and the clear zone, adjacent to the sealing membrane, containing mostly cytoplasm and a few organelles.

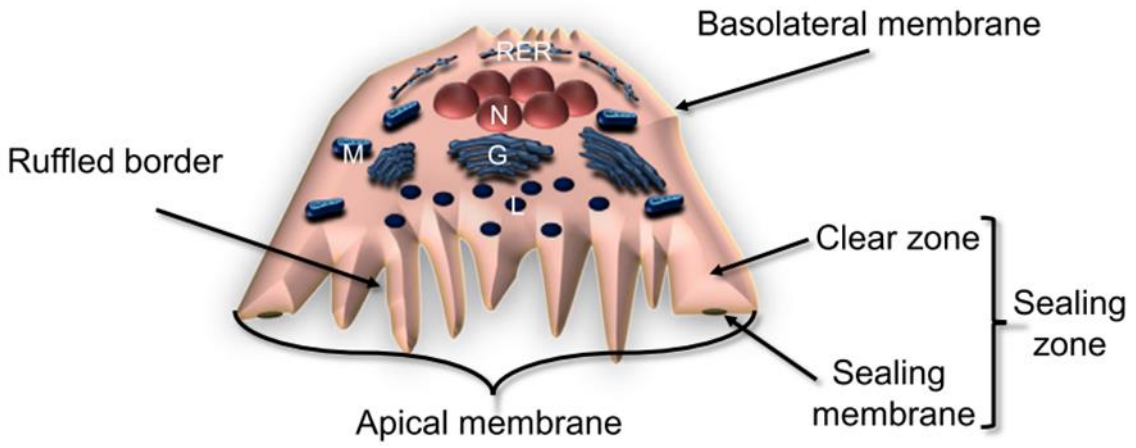

Figure 2- Schematic recreation of the plasma membrane domains of an osteoclast and the organelle distribution inside the cell. N: nucleus; M: mitochondrion; G: Golgi stack; L: lysosome; RER: Rough endoplasmic reticulum. Adapted from Cappariello *et al*.[11]

Podosomes are structures characterized by fast turnover, dynamic properties, rapid regulation and likely digestive capacity. Crucial components of the podosomes include: actin microfilaments, actin—binding proteins, adhesion proteins, adapter proteins, signalling proteins, tyrosine kinases and integrin receptors. Furthermore, actin rings are a hallmark of the resorbing osteoclast as well as a phenotypical characteristic. The integrin receptors, specially $\alpha_1\beta_2$, $\alpha_v\beta_3$ and $\alpha_v\beta_5$, serve as anchor proteins (by binding microfilaments to the extracellular matrix) and as receptors of several pathways capable of signalling the cells by numerous ways, such as calcium mobilization, adapter protein, non-receptor tyrosine kinase and small GTP-binding protein recruitment and activation. Alongside the sealing membrane is located the ruffled border, facing the area of bone to be resorbed. The ruffled border contains two subdomains named "fusion zone" and "uptake zone". While the "fusion zone" is responsible for allowing vesicular fusion to insert ion transporters into the ruffled border and secrete lysosomal enzymes, the "uptake zone" is implicated in taking in products generated during bone resorption. The above mentioned structures help forming the "resorption lacuna", situated underneath the ruffled border, and thoroughly set apart by the sealing membrane[11].

The "resorption lacuna" exists as an extracellular mechanism that sets up bone degradation. This mechanism is necessary because the large area of bone to be degraded makes it unsuitable for intracellular digestion. Even though the fusion of mononuclear precursors, as part of osteoclast differentiation, greatly increases cell size, this is not sufficient to guarantee intracellular degradation. This resorption compartment is characterized by low pH and high calcium concentration[12]. Acidification of the resorption lacuna is essential for demineralization of the bone matrix (by dissolving the HA), exposure of the organic components, mainly collagen I, and subsequent degradation. The mineral dissolution is supported by molecular mechanisms of proton release by the V-H^+-ATPase, located within the ruffled border, as well as the $2CL^-/1H^+$ antiporter, which assures the charge balance. Other players have been found to contribute to the extracellular acidification of the resorption lacuna, namely the carbonic anhydrase type II, the anion C^-/HCO_3^- exchanger and the PLEHKM1 protein. These intermediaries are involved in the accelerating the conversion of CO_2 in H_2CO_3, preventing cytoplasmatic alkalinisation and vesicular trafficking to the ruffled border, respectively[13–15]. After matrix demineralization, the degradation of the organic components ensues by the release of lysosomal enzymes, noticeable by the presence of mannose-6-P receptors, crucial for trafficking of lysosomal enzymes.

The most studied are Cathepsin K and tartare resistant acid phosphatase (TRAcP). Genetic mutations on Cathepsin K gene result in pycnodysostosis, a lysosomal storage disorder characterized by short bones, delayed sutures and deformities, besides increased bone density and fragility. While Cathepsin K is responsible for collagen I degradation, the function of TRAcP is not fully understood. It is known to be converted to an ATPase by enzymatic cleavage and its substrates include transforming growth factor β (TGF-β) receptor-interacting protein (TRIP-1)[16]. However, it has been reported that deletion of TRAcP in mice causes skeletal deformities, suggesting that TRAcP is both important during endochondral ossification and bone remodeling[17].

Bone Remodeling

Bone remodeling is a complex event by which old bone is systematically replaced by new tissue. This process is due to the role and interaction between key players of the bone microenvironment: osteoclasts, osteoblasts and osteocytes[7,9]. The close collaboration between these cells is described as the "Basic Multicellular Unit" (BMU). The remodeling cycle involves three consecutive stages: resorption, reversal and formation. Resorption is initiated through the migration of hemopoietic myelomonocytic precursors to the resorption site, followed by fusion and attachment of the newly formed osteoclasts to the bone surface. Soon after osteoclastic resorption, during the reversal phase, mononuclear cells appear on the bone surface and prepare it for new osteoblasts to set bone formation and supply signals for osteoblast differentiation and migration. Subsequently, the formation phase takes place with osteoblasts laying down bone until the resorbed one is ultimately replaced by new. After the bone formation phase is concluded, flattened lining cells cover the surface and a long resting period takes place until a new bone remodeling cycle is initiated[9]. The interaction between cells from osteoblastic and osteoclastic lineage demonstrates a coupling mechanism between bone resorption and formation. The stage of osteoclast formation is strongly driven by local factors secreted by nearby cells, specially osteoblast-lineage cells (preosteoblasts, mature osteoblasts, lining cells and osteocytes) and cytokines derived from other cells, such as immune cells within the bone marrow. As mentioned above, the interaction between the RANK receptor and its ligand is responsible for the activation, differentiation and fusion of osteoclast precursors, thereby initiating the process of resorption[9]. On the other hand, the production of the decoy receptor OPG, mainly by osteoblast lineage cells blocks the effects of RANKL. Bone resorption is therefore regulated through the inhibitory action of OPG on the final differentiation and activation of osteoclasts and by inducing their apoptosis. Since OPG is not incorporated into bone matrix, its effects on bone resorption are reversible[9].

However, the osteoblast-osteoclast (Figure 3) interplay is not limited to the dynamic between RANKL and OPG. Other molecules expressed by osteoblasts, besides OPG, inhibit osteoclast formation: Ephrin2/EphB4 and Sema3A. Zhao *et al.*[18] showed a bidirectional regulation process between osteoclasts and osteoblasts mediated through osteoclasts' Ephrin2, a transmembrane ligand, and osteoblasts' EphB4, a tyrosine kinase receptor. The authors reported that osteoblasts can inhibit osteoclast

formation through Ephrin signalling that down-regulates c-Fos and NFATc1 expression. On the other hand, signalling via Eph stimulates osteoblast differentiation by inhibiting the small GTPase, RhoA. Moreover, EphB4 signalling is an inducer of osteogenic regulatory factors such as Dlx5, Osx and Runx2[19]. More studies have implied other molecules, secreted by osteoblasts, with inhibitory action on the differentiation of osteoclasts, as is the case of Sema3A[8]. Sema3A is a part of a group of axonal growth cone guidance molecules called semaphorins. Hayashi *et al.*[8] demonstrated that Sema3A inhibited osteoclastogenesis through the regulation of DAP12-induced ITAM signalling, in which Nrp1 may compete with TREM2 for PlxnA1[19]. Besides interfering with osteoclast formation, osteoblasts can also promote apoptosis of osteoclasts. Although through different activation mechanisms, induction of apoptosis is via Factor associated suicide ligand (FasL).

The osteoclasts also play a role in regulating the activity of osteoblasts. Its inhibitory action on bone formation is conducted through a few molecules: D2 isoform of vacuolar (H+) ATPase (v-ATPase) V0 domain (Atp6v0d2); semaphorin 4D (Sema4D); and sclerostin.

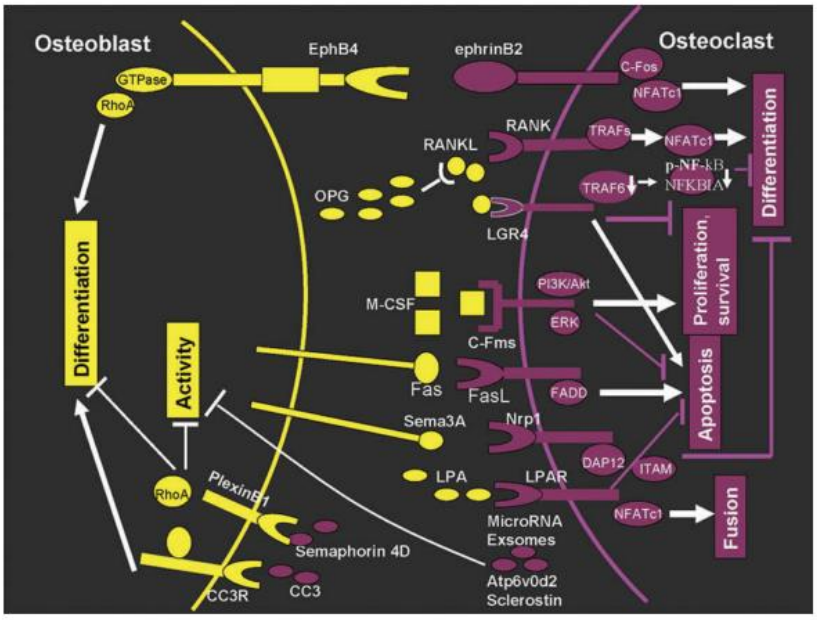

Figure 3-The schematic presentation of osteoblast–osteoclast interactions. Adapted from Chen *et al.*[19]

Atp6v0d2 is highly expressed in osteoclasts, but its functional importance is unclear. However, studies have reported that *Atp6v0d2* deficient mice displayed increased osteoblast and bone formation as well as impaired osteoclast maturation. Furthermore, the authors hypothesized the augmented osteoblast activity to be due to extrinsic factors produced by mutant osteoclasts or their precursors, since osteoblast differentiation related gene expression remained stable[19,20].

The inhibitory action of Sema4D is due to its interaction with Plexin-B1, expressed by osteoblasts. Studies in *Sema4D* deficient mice showed significant increases in bone mass, trabecular thickness, bone strength, bone formation, and osteoblast surface compared to wild-type. Plexin-1 is remarkably expressed during osteoblast differentiation and forms a complex with erythroblastic leukemia viral oncogene homolog 2(ErbB2) in osteoblasts. It was found that biniding of Sema4D to this complex might attenuate IGF-1 signalling and affect osteoblast motility through RhoA activation[19].

The inhibitory action of sclestorin, expressed in human long bones, cartilage and osteocytes, has already been described above, in the osteocyte section. Kusu *et al.*[21] reported the expression of sclestorin in mouse osteoclasts of in developing bones of mouse embryos, and further showed that it bound to BMP6 and BMP7, inhibiting osteoblastic activity *in vitro*. Another study[22] has shown that the expression of sclestorin in older mice osteoclasts and that their conditioned medium repressed mineralization of bone marrow stromal cells. These effects were reversed after antibodies specific to sclestorin were added to the cultures[22].

However, the effects of osteoclasts on the activity of osteoblasts is not limited to inhibitory ones. For instance, Complement component 3a (CC3a) has been reported[23] to stimulate osteoblast differentiation *in vitro*, through a co-culture model of osteoblasts and mature osteoclasts. Furthermore, in ovariectomized mice, CC3a expression in bone was increased with exacerbated osteoclast activation. In addition, when a CC3a antagonist was administered, stimulation of bone formation was impaired[23]. Other molecule called Cthrc1 secreted by mature osteoclasts during bone resorption may stimulate osteogenesis[19]. Osteoclast-specific deletion of Cthrc1 has been shown to hinder bone formation and consequently cause osteopenia. Moreover, these knockout mice displayed low bone mass, low bone formation rate, and other structural abnormalities[19,24].

Bone Formation

Skeletal development demands a well-defined and meticulous organization between several events: cellular growth, differentiation and apoptosis, ECM remodeling and angiogenesis. There are at least two different processes that guide bone formation: endochondral and intramembranous ossification[25]. Prior to either of these osteogenic events, a phenomenon named mesenchymal condensation determinates both the position of skeletal elements they represent and their basic shape. Condensation is the crucial event in the development of skeletal and other mesenchymal tissues[26]. It takes place when formerly diffused mesenchymal cells aggregate or condensate, which is the first sign of formation of a skeletal element, and its timing, position, and shape are determined by *Shh*, *Bmp* (BMP-2-5, BMP7), *Fgf*, and *Hox* genes. Mesenchymal cells undergoing condensation can either differentiate into chondrocytes or osteoblasts. While the commitment to the chondrocytic lineage occurs in sites of endochondral ossification, the differentiation into osteoblasts takes place in a context of intramembranous ossification and is further detailed within this topic.

1. Intramembranous Ossification

Intramembranous ossification occurs through direct differentiation of mesenchymal cells into osteoblasts, after mesenchymal condensation. This process of ossification, as well as endochondral ossification, happens concomitantly with vascular ingrowth. Together with the capillary invasion, mesenchymal stem cells also invade the mensenchymal zone to differentiate into osteoblasts. The path in cell fate is regulated by the canonical Wnt signalling, itself caused partially by sonic hedgehog. In the lack of Wnt signalling, mesenchymal cells differentiate into chondrocytes. Amid prechondrogenic condensation, the increase of intracellular cAMP levels and cell-cell interaction are believed to intervene in the upregulation of chondrogenic genes. The transcription factor Sox9 strongly induces the expression of genes needed for cartilage formation, namely collagen II (*Col2a1*) and aggrecan (*Agc*), and upon phosphorylation by protein kinase A (PKA), its DNA binding and transcriptional activity is increased. Sox9 expression is initially observed in mesenchymal chondroprogenitor cells and

reaches high levels of expression in differentiated chondrocytes. Cells lacking *Sox9* expression do not commit to cartilage lineage but remain as a close mesenchyme with no chondrocyte-specific markers. This exclusion mechanism takes place during mesenchymal condensation of chondrogenesis and the important role of Sox9 identifies it as the first transcription factor essential for chondrocyte differentiation and cartilage formation[27]. A key regulator of intramembranous ossification is the gene runt-related transcription factor 2, Runx2. Expression of this transcription factor, in areas of membranous ossification, is a marker for cessation of condensation growth, leading to differentiation into osteogenic cells. Since the expression of Runx2 is dependent on Wnt signalling, high levels of ß-catenin are detectable in mesenchymal cells. Runx2 further induces the expression of another transcription factor named Osx. Together, these two growth factors play crucial roles in differentiation of osteoblasts from mesenchymal cells[27].

Osteoblasts then secrete bone matrix mainly composed collagen type I, but also non-collagenous, extracellular matrix proteins deposited along with an inorganic mineral phase. During this process, osteoblasts eventually become entrapped in the bone matrix, hence named osteocyte, the mature bone cell[28]. Intramembranous bone formation is responsible for the development of the cranial vault flat bones, as well as cranial suture lines, some facial bones and parts of the mandible and clavicle[27].

2. Endochondral Ossification

Endochondral ossification (Figure 4[29]) is a complex multistage event comprised of sequential formation and degradation of cartilaginous structures that provide a template for the imminent bone. This type of bone formation happens not only during skeletogenesis, but also throughout postnatal growth, bone remodeling and fracture repair[27]. Like the initial events of intramembranous ossification, the first step includes the condensation of mesenchymal precursor cells resulting in the creation of the bone template. The differentiation of mesenchymal precursors is followed by hypertrophy of the newly formed chondrocytes within the centre of the diaphysis. Preceding hypertrophy, chondrocytes secrete collagen II, aggrecan and other matrix molecules distinctive of hyaline cartilage ECM. On the other hand, upon hypertrophy, chondrocytes express collagen X, leading the mineralization of the surrounding matrix, signalling adjacent cells of the perichondrium to differentiate into osteoblasts and promoting the invasion of blood vessels. While doing so, these cartilage cells also induce sprouting of angiogenesis from the perichondrium through expression of

vascular endothelial growth factor (VEGF), that binds to its respective receptors VEGFR1 and VEGFR2, both expressed by endothelial cells (ECs). This VEGF-mediated blood vessel invasion promotes the recruitment of chondroclasts, osteoclasts and osteoblasts, as well as the delivery of nutrients and proapoptotic signals. The capillary invasion of the perichondrium that surrounds the future diaphysis transforms it into the periosteum.

Meanwhile, following differentiation and maturation, the osteoblasts secrete collagen I and other bone-specific molecules, such as ALP. Subsequently, upon mineralization by intramembranous ossification, these events will lead to the formation of the bone collar, the cortical bone. Once the bone collar is formed, osteoclasts invade the cartilage template and digest the matrix previously synthesized by the hypertrophic chondrocytes. The primary growth plates are soon after established and act as a steady source of cartilage conversion to bone and linear growth of the long bone throughout development and postnatally.

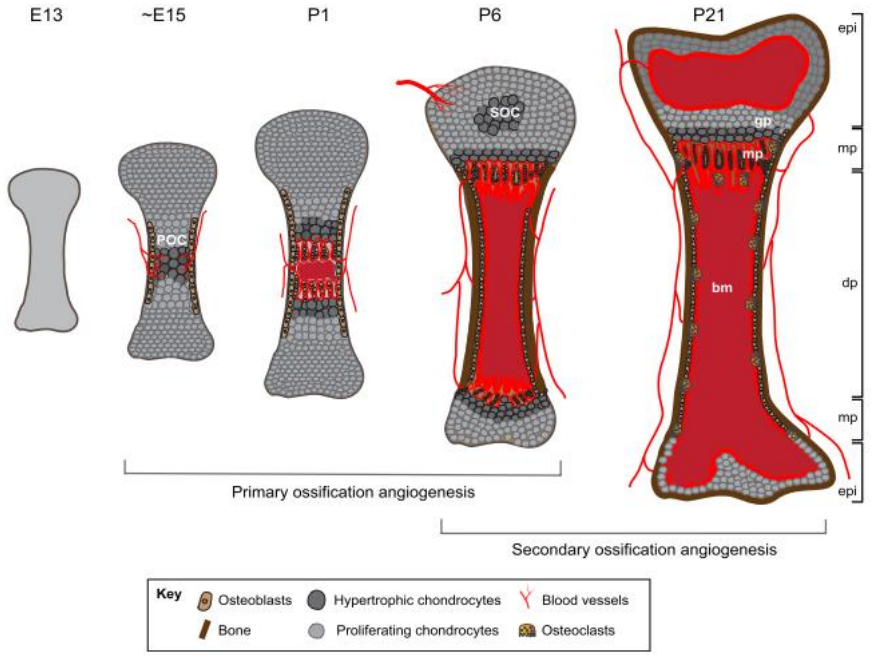

Figure 4-Schematic representation of endochondral angiogenesis. Prior to birth, mesenchymal condensation takes place, originating chondrocytes to form cartilage. Soon after, chondrocyte hypertrophy in the center of the primary ossification center (POC) leads to the secretion of pro-angiogenic factors that stimulate the invasion of blood vessels that extend within the growing bone and grow towards the epiphysis in both directions at postnatal day 1. Then, morphologically distinct capillary beds can be readily distinguished in the metaphysis and diaphysis. Blood vessels start to invade the epiphysis and contribute to the formation of the secondary ossification center. 21 days after birth, bone growth and vascularization are far advanced, and all major structures have been established. Adapted from Sivaraj and Adams[29].

The growth plate (Figure 5) is comprised of four different zones that, although different from each other, assemble a merging continuum[27]. The reserve zone is characterized for the predominance of randomly distributed chondrocytes, separated by large amounts of matrix composed of collagen II and proteoglycans. The cells from

this area eventually assume a discoid shape (previously nearly spherical) and are arranged into column-like structures, bringing together the proliferation zone. Through the proliferation of the chondrocytes, the cartilage anlagen elongate, mainly at its ends since it is where the cell proliferation is maximal. Ultimately, the chondrocytes from the proliferation zone enlarge, losing their discoidal shape while moving to the maturation zone (prehypertrophic chondrocytes). At this stage growth ensues through increases in cell size and not through cell division. Within the midsection, the chondrocytes undergo maturation, size enlargement (hypertrophy) and secret a matrix rich in collagen X. After depletion of glycogen stores, chondrocytes undergo apoptosis, leaving behind longitudinal lacunae separated by septae of cartilaginous matrix that become selectively calcified as well as broadly uncalcified transverse septae. Following these changes, new blood vessels enter the lower hypertrophic zone from the primary spongiosum and invade the transverse septae, whereas chondroclasts that accompany this erosive angiogenic process remove calcified cartilage. In the next chapter, we further analyse the role of angiogenesis in bone, highlighting the contribution of osteoclasts to the process and their interplay with ECs.

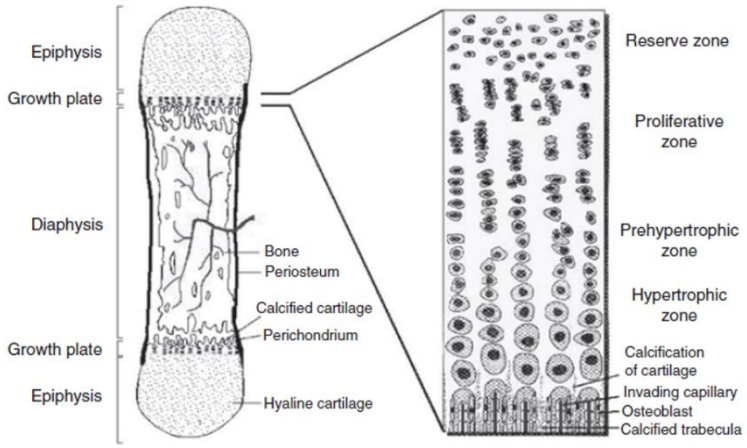

Figure 5- Formation and growth of long bones by endochondral ossification (right). Schematic representation of the organization of the mammalian growth plate (left). Adapted from Karaplis[27].

Angiogenesis and Osteoclastogenesis Coupling

Vasculature is essential for bone formation and remodeling, since it contributes for tissue homeostasis through supply of oxygen, nutrients, soluble factors and different cell types. In fact, the inability to develop a capable vascular structure within the bone tissue is related to several skeletal pathologies such as osteonecrosis, osteomyelitis and osteoporosis [30]. The formation of mature blood vessels during fetal development occurs in various phases. ECs differentiate from mesodermal progenitors and assemble to form a primitive vascular network; this vascular network then expands and remodels by angiogenesis, which represents a mechanism of sprouting from pre-existing blood vessels, to model highly branched ducts that supply nutrients and oxygen to the tissues of the embryo. The establishment of a functional vascular network demands maturation of recent vessels into arteries, veins and capillaries[31]. The microvascular circulation plays a key role in maintaining the homeostasis of resident stem cells and leading regeneration and repair of adult tissues[32].

Recent reports have shown that the skeletal system possesses heterogeneous and functionally specialized blood vessels. Bone capillaries were divided in two main subtypes: type H vessels, mainly present in the metaphysis of long bones and highly positive for CD31 and Endomucin ($CD31^{hi}Emcn^{hi}$); type L, and extension of type H vessels, form sinusoidal vessels within hematopoietic bone cavity and express lower levels of CD31 and Endomucin ($CD31^{lo}Emcn^{lo}$). These vessels also display differences regarding interaction with cells, since type H vessels display high proliferative activity and secrete factors that regulate osteoblast function and chondrocyte proliferation. Additionally, osteoprogenitor cells position themselves around type H vessels, but not type L[32] (Figure 6[33]).

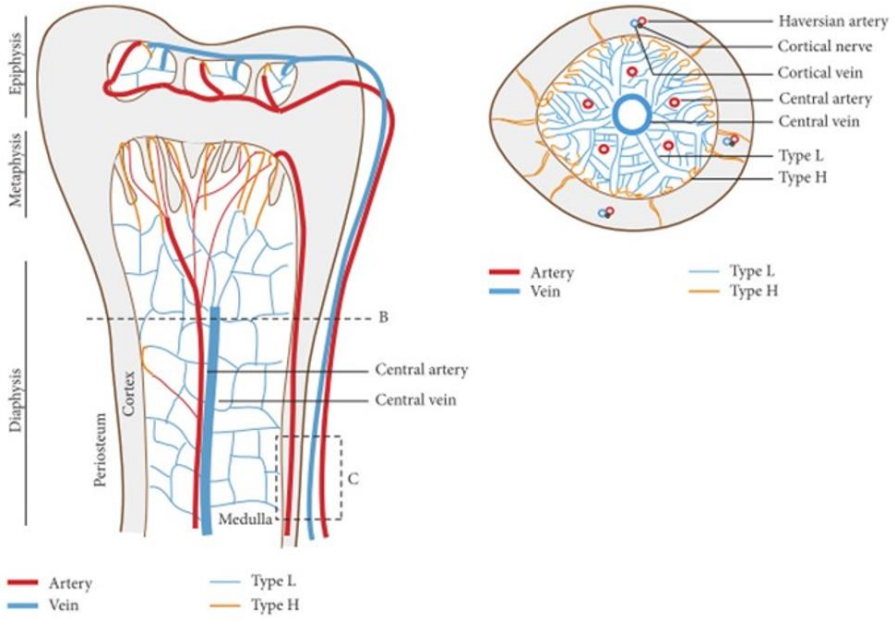

Figure 6- Blood vessel organization in bone: longitudinal view (left) displays arrangement of arteries, veins, and capillaries in different long bone areas. Arteries disperse into smaller arterioles and terminate in type H capillaries. Type H capillaries are located near osteoprogenitors in the metaphysis and endosteum regions. Type L capillaries are sinusoidal vessels terminating in the central vein. Transverse view (right) shows bone vascular organization in cortical and medullary regions of long bone. Adapted from Ramasamy[33].

During endochondral bone development, the reorganization of the avascular cartilage template into remarkably vascularized bone and marrow tissues is set off by the invasion of blood vessels into the hypertrophic chondrocyte core. This process of neovascularization of the cartilage anlagen is associated with its deterioration through the apoptosis of differentiated chondrocytes, matrix digestion by proteolytic enzyme activity and resorption of the calcified cartilage by osteoclasts and chondroclasts. The cavity created through these events soon becomes the site occupied by osteoblasts and subsequent bone formation. This region is called the primary ossification centre. At the chondro-osseous junctions (edges of the primary ossification centre), the same basic cellular mechanisms take place and gradually replace cartilage with metaphyseal bone [31]. Thus, it is noticeable that angiogenesis plays an important role throughout endochondral formation. On the other hand, its role is also noticeable in intramembranous ossification, process by which craniofacial bones are formed. VEGF plays a major role throughout this type of bone development. Its loss is linked with impaired bone skull formation and delayed fracture healing[32]. During intramembranous regeneration, when exposed to hypoxia, in the initial phase of inflammation, osteoblasts secrete various factors such as VEGF, *via* HIF-1α pathway, stimulating endothelial cell migration and proliferation and vessel permeability. These new vessels allow the delivery of nutrients, oxygen and minerals essential for osteogenesis, as well as osteoprogenitors for the site of injury. Moreover, ECs also produce osteogenic

factors capable of promoting osteoblast differentiation. Additionally, osteoblasts will also release angiogenic factors (PDGF-BB and VEGF), thereby supporting angiogenesis through a positive feedback cycle[32]. VEGF also has effect on other cell populations related with the bone microenvironment. In bone repair, during the inflammatory phase, VEGF induces the recruitment of immune cells. Furthermore, it also influences osteoclast function since M-CSF, RANKL and VEGF are necessary for their recruitment and differentiation. In osteopetrotic mice, deficient in osteoclasts, monocytes and macrophages, VEGF delivery increased osteoclastogenesis and bone resorption[34]. Other study has shown that VEGF overexpression is the source of excessive osteoclast recruitment and bone resorption in tissue-engineered osteogenic constructs[35].

Although there has been a growing number of reports focused on the study of the blood vessel formation and function in bone, the interplay between osteoclasts and ECs is yet to be fully understood. In 1993, Zaidi *et al*. reviewed the role of ECs in osteoclast control, focusing on reported effects of endothelial cell-derived products, namely endothelins, nitric oxide and reactive oxygen species, as regulatory agents on osteoclasts. The authors reported that both endothelin and nitric oxide inhibit bone resorption. Whereas endothelin causes impaired margin ruffling, nitric oxide promotes cell retraction. Contrarily, reactive oxygen species enhance osteoclast activity. It was later reported that inflammatory cytokine activation of human vascular endothelial cells (HMVEC) led to a sustained upregulation of RANKL, opposed to a more transient expression of OPG[36]. As a result, *in vitro*, HMVEC displayed an increased ability to stimulate the co-culture development and activity of mature bone pit-resorptive osteoclasts from human monocytic precursors. Moreover, *in vivo,* RANKL expression was upregulated on vascular endothelial cells (VEC) adjacent to resorbing osteoclasts and sites of bone remodeling, implying inflammatory-activated VEC may help enhancing localized bone loss via RANKL-mediated effects on pre-osteoclasts and osteoclasts[36].

Further co-culture studies have been published more recently. An indirect co-culture model between mice endothelial progenitor cells (EPCs) and OC precursors showed an enhancement of survivability, migration and differentiation of the OC precursors, caused by the EPCs[37].The authors state these effects could be attributed to the secretion of VEGF-A, SDF-1 and TGF-β1: VEGF-A enhances osteoclast survival and bone resorption; SDF-1 promotes chemotactic recruitment, development and survival of pre-OC; and TGF-β1 modulates growth and induces osteoclast chemotaxis. Moreover, it was also shown that the synergistic effect of these three factors induces osteoclastogenesis without RANKL and M-CSF stimulation, although not as effective[37].

However, other reports also attribute an inhibitory effect on OC differentiation to ECs. In 2002, Chikatsu *et al.*[38] observed that osteoclastogenesis was inhibited during the co-culture of VEC and bone marrow macrophages, without cell-cell direct contact, although the mechanisms behind these effects remained to be elucidated. Following this work, Enoki *et al.*[39] showed that VEC inhibit osteoclast differentiation via netrin4 (Ntn4), a secreted protein member of the laminin superfamily and are involved in axon migration, lymphangiogenesis and vascularization. *In vitro,* the authors observed that the co-culture of VEC with bone marrow macrophages in a transwell system, strongly inhibited osteoclast formation. This effect was supressed once specific anti-Ntn4 antibodies and siRNA against *Ntn4* were added to the co-cultures. Moreover, when Ntn4 was added to bone marrow macrophages cultures, in the presence of RANKL and M-CSF, RANKL-induced osteoclast formation was inhibited. *In vivo,* the authors showed that the administration of Ntn4 to osteoporosis mouse model prevented bone loss, corroborating the previous *in vitro* result. Since vascularization is an important process to all regions of the bone, the authors hypothesized that VEC produce Ntn4 and inhibit osteoclast differentiation in pathophysiological conditions, such as bone fracture or overloading, to balance the effect of RANKL stimulation, produced by osteoblasts[39].

It is still not well understood whether osteoclasts stimulate angiogenesis by secreting soluble factors or by releasing matrix-bound factors, or if both mechanisms are present[40]. In multiple myeloma, both osteoclastic activity and angiogenesis, promote disease progression and bone destruction. The enhanced angiogenesis observed is thought to be a result of simultaneous action of both myeloma cells and osteoclasts[41]. Through angiogenesis assays, using osteoclast conditioned medium, Tanaka *et al.*[41] have implied a paracrine effect of osteoclasts on ECs, caused by osteopontin (this study is further detailed in the Results and Discussion section). Even though other authors have questioned these results, these studies may have hinted a direct effect of osteoclasts on ECs[40].

Previous reports have implicated matrix metalloprotein-9 (MMP-9) as an angiogenic key player on a multistage carcinogenesis model[42], osteoclast invasion of long bone growth plate and VEGF-induced migration through release of matrix bound VEGF[43]. MMP-9, in adult bone is mainly expressed by osteoclasts. More recently, Cackowski *et al.*[44] aimed to determine the effect of osteoclasts and their secretion of MMP-9 on angiogenesis. In the report, the authors first studied if osteoclasts had any effect on angiogenesis *in vitro*, using a bone explant. It was observed that inhibition of osteoclast formation and activity through OPG had a negative impact on angiogenesis, whereas stimulation of osteoclast activity through PTHrP enhanced

angiogenesis. PTHrP increases osteoclatogenesis primarily through increased RANKL expression on osteoblasts. They concluded that the increased angiogenesis was due to osteoclast activity because the PTHrP proangiogenic effect was blocked in the presence of OPG. Further *in vivo* examination showed augmented angiogenesis when osteoclast activity and formation was stimulated through RANKL and PTHrP. The authors then studied the mechanisms responsible for osteoclast stimulation of angiogenesis and identified MMP-9 as an important agent in this process. Metatarsal explants of *Mmp9*$^{-/-}$ mice showed no angiogenic nor resorptive effects when stimulated with PTHrP. Moreover, the proangiogenic, bone resorptive and osteoclastogenic impact of RANKL were decreased in *Mmp9*$^{-/-}$ calvaria *in vivo*. Based on observations regarding number of vessels, osteoclast number, activity and migration to sites where angiogenesis occurs, between *Mmp9*$^{-/-}$ and WT mice, the authors suggest a mechanism (Figure 7) by which osteoclast-stimulated angiogenesis and osteoclast migration is connected to MMP-9 and its ability to release heparin-binding isoforms of VEGF-A from the ECM. The action of MMP-9 is important for osteoclast recruitment into the primary ossification centre and *Mmp9*$^{-/-}$ mice display delayed vessel invasion into the primary ossification centre.

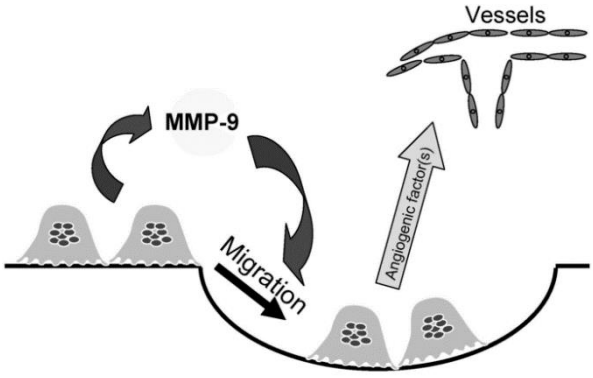

Figure 7- Role of MMP-9 in osteoclast-stimulated angiogenesis. In the model presented by Cackowski et al., osteoclasts release MMP-9, which induces osteoclast migration to increase local osteoclast numbers and activity. The osteoclasts secrete factors that stimulate capillary invasion. Adapted from Cackowski et al.[44]

Xie *et al.*[45] showed that preosteoclasts, immature progenitors of osteoclasts, stimulate angiogenesis and osteogenesis during bone remodeling through the secretion of platelet derived growth factor-B (specifically the homodimeric form of the growth factor, PDGF-BB)[46] (Figure 8). PDGF-BB is a mitogenic and chemotactic agent and stimulates the proliferation and migration of numerous types of cell types, namely MSCs, pericytes and fibroblasts, through binding with the receptor PDGFR-β. Using the Cre-lox technology, the authors depleted the *Pdgfb* gene in osteoclast lineage-cells. It

was observed that the osteoclast lineage is a major source of PDFG-BB in peripheral blood and bone marrow. Moreover, these mutants showed reduced bone vasculature, including fewer $CD31^{hi}Emcn^{hi}$ ECs, besides impaired trabecular bone mass, cortical bone thickness and bone formation, PDGF-BB exerts a regulatory effect on MSCs, essential for osteoblast formation and consequently osteogenesis. MSCs are also a source of VEGF, a key regulator of angiogenesis in several tissues. Thus, it is likely that some of the beneficial effect of PDGF-BB secreted by POC on vascularization and bone formation may be mediated by MSCs. In this study, it was also observed that PDGF-BB induced migration of bone marrow-derived EPCs.

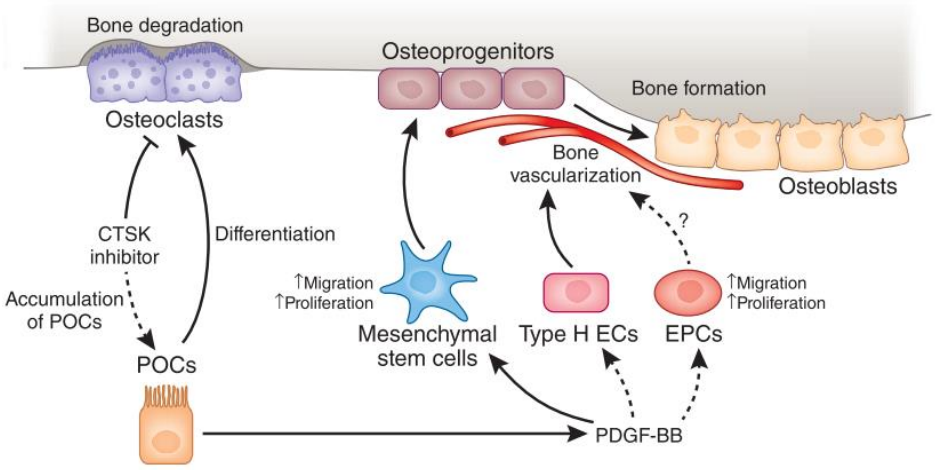

Figure 8- Osteoclast precursors secrete the growth factor PDGF-BB, leading to increased migration and proliferation of mesenchymal stem cells, which originate osteoprogenitor cells and subsequently bone-forming osteoblasts. POC- derived PDGF-BB is also crucial for the formation of CD31hiEmcnhi (type H) blood vessels in the bone. Adapted from Kusumbe and Adams[46].

Despite this close interaction between osteogenesis and angiogenesis, the cross talk between osteoclasts and ECs remains to be fully elucidated. While some studies show a positive effect of ECs on the survivability and proliferation of osteoclast precursors, its ability of inhibiting osteoclast activity has also been reported through molecules such as endothelins, nitric oxide and Ntn4. Osteoclasts have been shown to manifest angiogenic potential, but their mechanisms of action remain uncertain. A possible paracrine effect has been hinted through osteopotein, but further studies are required. Other reports have stated that osteoclasts can also promote angiogenesis through the release of matrix bound angiogenic factors, such as VEGF, via MMP9-mediated mechanism. Preosteoclasts also play a role promoting angiogenesis through the release of PDGF-BB, enhancing the formation of $CD31^{hi}Emcn^{hi}$ blood vessels. Nevertheless, further studies are required to unravel the complex interaction existing between angiogenesis and osteoclastogenesis.

Bone innervation

As displayed in the previous sections, bone remodeling, and consequently its homeostasis, is heavily regulated by hormonal, autocrine/paracrine signalling and mechanical processes. However, an increasing number of reports have unveiled a link between the nervous system and bone, by providing evidence of its influence on bone homeostasis[47]. Bone is a densely innervated organ, with nerves distributed across different anatomical sites of the bone and commonly located with the blood vessels, especially peripheral nerves. Some reports describe both sensory and autonomic fibres found in numerous areas of the bone such as vessels located within the periosteum, osteochondral junction of the growth plate, bone marrow, Volkmann's canals and attachment of the synovial membrane. Other studies report intensive networks of sensory and sympathetic nerve fibres mainly in areas of trabecular bone and less in cortical bone, bone marrow and epiphyseal growth plate[48]. Nerves distributed throughout the bone tissue perform two different functions: the first is the regulation of bony mechanical forces; the second is to provide trophic factors crucial for both structural and functional homeostasis. Moreover, studies involving bone denervation have reported impaired fracture healing, further underlining the relevance of the peripheral nervous system on bone turnover[49,50].

1. Nerve anatomy in bone

The cell bodies of afferent nerves are located in the dorsal root ganglion (DRG), which are connected to the Central Nervous System (CNS) via the dorsal spinal roots or the cranial nerves. The endings of sensory neurons in the bone tissue can either be free-fiber endings or encapsulated endings. Free nerve endings are unmyelinated, branched throughout tissues and capable of recognizing and transmit signals related to pain, temperature and mechanical stimuli. The encapsulated nerve endings are enclosed in non-neural fibrous capsules separating single afferent nerve endings in gelatinous material. These nerve endings are sensitive to low frequency vibrations.

Nerve fibers are distributed across the whole bone, including the periosteum, bone marrow and mineralized parts of the bone, mainly located at metabolically active sites (epiphysis and metaphysis). Although the total number of sensory and sympathetic fibers is the highest in bone marrow, the density of nerve fibers is highest in the periosteum, specifically in the fibrous connective tissue that surrounds the

surface of mineralized bone. Moreover, the nerve fibers in bone marrow arise from the periosteum and the nutrient foramen and then disperse reach all the bone marrow. The vast majority of nerve endings are distributed alongside arteries and capillary blood vessels, but some are dispersed along the bone marrow[51].

2. Neuropeptides and Bone Remodeling

Several neuropeptides, found in nerve fibers, were described to interfere with bone metabolism. From those, calcitonin-gene related peptide (CGRP) and substance P (SP), mostly originated from sensory nerves, have been target of extensive research and are amongst the most impactful[51].

CGRP is comprised of 37 amino acids and is the result of tissue specific alternative processing of the primary RNA transcripts of the calcitonin gene. It is a neuropeptide commonly found in sensory neurons innervating the skeleton. Several studies report CGRP-positive nerve fibres in different areas, at different stages of development: experimental models in rat femurs showed CGRP-positive nerve fibres in the metaphysis, during bone metabolism, 10 days after birth, and even more abundantly around the epiphysis, facing the growth plate; another study reported the presence of CGRP-immunoreactive nerve fibres within the outer layer of articular cartilage, in contact with chondrocytes in the knee joints of both mature and infant rats[48]. CGRP affects both osteoblasts and osteoclast. It seems to exert a direct action on osteoblasts by enhancing cAMP production, thereby stimulating their proliferation, production of growth factors and cytokines, collagen synthesis and, ultimately, bone formation. Regarding the effects on osteoclasts, studies *in vitro* indicate that CGRP may inhibit resorption, like calcitonin, but less potent. *In vitro* studies have shown CGRP to have an inhibitory effect in human osteoclast-like cells proliferation, through a cAMP mechanism[52]. *In vivo* studies using αCGRP$^{-/-}$ (αCGRP, also known as CGRPI has been considered that the principal form found in the central and peripheral nervous system; βCGRP, or CGRPII, is the second isoform and is mainly present in the enteric nervous system[53]) mice have not reported resorption deficiencies[54,55].

SP is another neuropeptide found in the nerve fibres, although fewer compared with those containing CGRP. SP fibres innervate the medullary tissues of the bone and the periosteum. Although the role of SP is the stimulation of cAMP production by osteoblastic cells, Goto *et al.* [56] showed that SP enhances osteoclasts' activities, proven by the expression of neurokinin-1 receptor, through which SP induces signal transduction. Furthermore, Mori *et al.*[57] reported that the addition of SP to rabbit

cultured osteoclasts enhanced their bone resorption capability, possibly by elevation of [Ca^{2+}], by 170%, whereas the addition of SP antagonists reverses these effects.

While there is extensive research on the mechanisms by which bone cells respond to neural factors and their influence on bone homeostasis, there are fewer reports studying how bone cells, mainly on BMSCs, support the presence and sprouting of nerve fibres within the bone microenvironment[51]. Given the already exiting reports about the role of osteoclasts on the activation of nociceptors under pathological conditions, specifically in cancer-associated bone pain, recently, Neto *el al.*[58] aimed to uncover the contribution of osteoclasts to nerve fibres outgrowth by exposing DRG to secretome of mature osteoclasts within microfluidic devices. The study proved that osteoclastic lineage does promote greater axonal outgrowth then bone marrow stromal cells, known to possess high neurotrophic capacity. Osteoclast mediated axonal outgrowth was shown to be neurotrophin-independent but implicates epidermal growth factor receptor (EGFR)/ErbB2 signalling[58].

3. Coupling between angiogenesis and innervation

Both nerve fibers and blood vessels are distributed across Harversian and Volkmann's canals in the bone. Besides the anatomical proximity, these are also functionally linked, demonstrating a synergistic effect between vascularization and innervation important during bone development and healing. While blood vessels provide oxygen and nutrients that enhance the formation of a nerve network, sensorial neuropeptides from nerve fibers influence angiogenesis and eventually promote bone healing. Both CGRPI and SP present vasculogenic properties. Despite acting on different vascular receptors, but both promote endothelial cell proliferation, migration and improve\ angiogenesis[59]. CGRPI interacts with cells through CGRPI receptor and receptor activity modifying proteins (RAMPs) that are expressed by ECs and osteoblasts. CGRPI exerts a direct effect on vascularization by modulating blood vessel smooth cells and ECs activity, playing a key role in the dilatation of blood vessels[51]. SP induces migration of MSCs to injury site and promoting production of VEGF, not only essential for angiogenesis, but also beneficial to bone formation. Another neuropeptide with angiogenic action is β-nerve growth factor (β-NGF). β-NGF is a neurotrophin that plays an important role in promoting neurotrophic and neurotropic effects in sympathetic neurons, but also may influence survival and function of ECs by autocrine/paracrine mechanisms[51]. Its biological effects are directly depending on its interaction to TrkA, a transmembrane tyrosine kinase, the specific receptor for NGF. Recently, Tomlinson *et al.*[60], by using mouse models, have shown

that sensory nerve axons originated from the DRG innervate sites of incipient bone formation in response to NGF expression and that disruption of TrkA signalling in these nerves hinders axon ingrowth, delays vascularization and ossification of bone[60].

In vitro bone models

In vitro models are important tools to mimic *in vivo* systems and have evolved tremendously to improve its complexity in order to reproduce physiological and pathological conditions. Co-culture models are of extreme importance to help on the understanding of cellular and molecular interaction mechanisms within controlled systems.

The use of microfluidic platforms to assemble *in vitro* models has been increasing rapidly across different research fields due to their low manufacture price, easy manipulation. Although different materials may be utilized to produce microfluidic devices, the most common is an elastomer called polydimethylsiloxane (PDMS), characterized for being optically transparent, as well as gas and vapour permeable. The prevalence of PDMS as the main material for the fabrication of microfluidic devices is related to different factors, from which it is important to highlight its low price, easiness of use and flexibility regarding modification of surface properties[61]. In addition, through soft lithography, different designs can be patterned into PDMS, allowing for researchers to create and tweak various architectures depending on the end goal of their research. The possibility of controlling microphysiological cues, such as shear stress or oxygen levels, as well as the set-up of co-cultures of different cell types, under 2D or 3D conditions, have made microfluidic platforms useful and innovative tools in the context of biological research[4,62]. Its use is widespread across studies of different tissues and different strategies have been employed to achieve models that mimic physiological interactions within tissues and organs in simple, yet functional, microfluidic devices, often called organ-on-a-chip[63].

Microfluidic devices have also been a relevant tool in the context of neurobiological research. The first microfluidic platform specifically designed toward neurobiological studies introduced a two-compartment device that allowed for axonal projection across different compartments[64]. This microfluidic design aimed to recreate axon guidance processes that happen upon establishment of complex neuronal networks in response to multiple signals from the surrounding matrix towards the sites of synaptogenesis[62]. Hence, these platforms allow researchers to isolate axonal fractions and study parameters that guide axon outgrowth and synapse formation. A particularly useful application of these *in vitro* tissues, similar to other biological fields, is the assemble of co-culture models that provide insight how neurons

communicate with non-neuronal tissues in both homeostatic and pathological conditions. With this in mind, several co-culture studies have been reported between different central or peripheral nervous system and other cell types, such as stem cells, cancer, bone, muscle and glial cells (Figure 9).

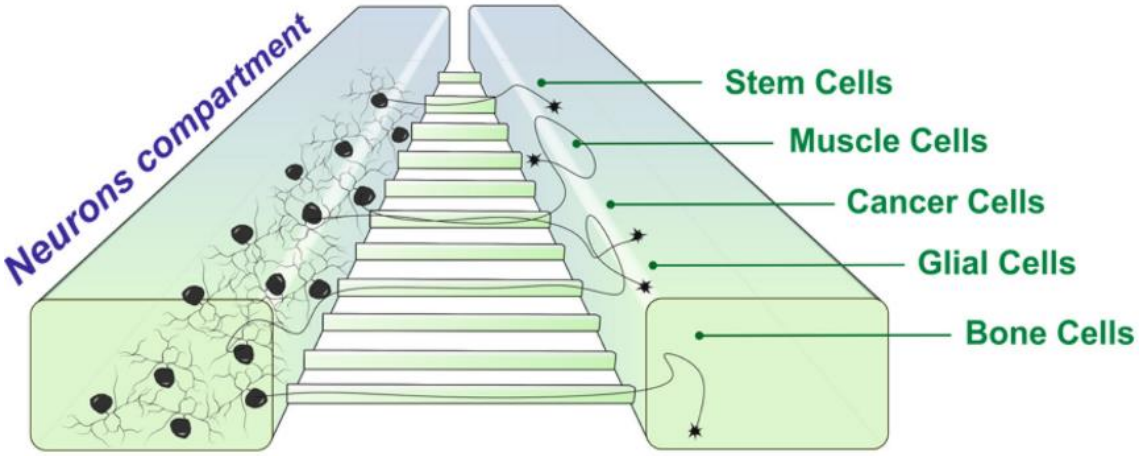

Figure 9- Schematic representation of microfluidic platforms showing axonal projection from a neuronal compartment (left) towards a separated compartment (right) where different cell types can be seeded. Adapted from Neto, Leitão *et al.*[62]

As displayed throughout the previous sections, innervation plays a major role in bone homeostasis. With emphasis on the peripheral nervous system, several reports have been published to study the interaction between sensory neurons. Neto *et al.*[65] reported a functional *in vitro* co-culture model of sensory neurons and mice bone marrow derived-osteoblasts. Within this study, the authors were able to culture DRG and osteoblasts in different compartments, where the bone cells were culture in either 2D or 3D set-up, in a bone mimicking microenvironment (Figure 10). Furthermore, a close interaction between both cell types was observed, confirmed by the existence of mature neurites. The authors also developed a method of quantifying axonal growth through a MATLAB-based algorithm, later used in a recent study published by the same team.

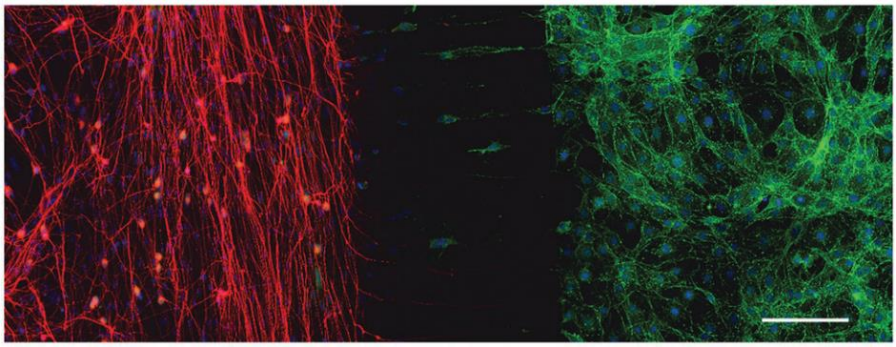

Figure 10- Cocultures of Dorsal root ganglion neurons (red) and osteoblasts (green). Adapted from Neto, Leitão *et al.*[65]

A similar culture model was later assembled, but with no cells in the axonal compartment. Instead, sensory neurons were exposed to the secretome of mature osteoclasts, already discussed above[58].

As highlighted previously, vascularization plays a major role in bone development and homeostasis. Through skeletal blood vessels, the various cell populations that inhabit the bone microenvironment are supplied with oxygen, nutrients, growth factors, hormones and calcium and phosphate, crucial for matrix mineralization. In addition, the bone cells and ECs communicate reciprocally to regulate both osteogenic and angiogenic functions. Another important function is the preservation of stem and progenitor cell niche supported by the bone marrow vascular system[66]. Despite the close relation between peripheral nerves and blood vessels, both anatomical and functional, peripheral innervation microfluidic models do not include ECs. Nevertheless, researchers have employed different strategies to recreate vascular structures within microfluidic devices, including bone vascularized models.

Microfluidic platforms have been an attractive tool for the development of *in vitro* vasculature models because they allow the culture of vascular cells in patterned systems that mimic the geometry of microvascular systems found *in vivo*, under rigorous controlled flow conditions and seeded within scaffolds that provide a suitable microenvironment for the formation of capillary structures[67,68]. The patterning of this engineered vascular networks can be achieved developing hollow channels within different scaffolds, that will later harbor vascular cells to form the intended and enclosed vascular structures. However, this strategy often hinders vascular remodeling and nutrient transport due to the dense and impassable nature of the materials that constitute the microfluidic device. This obstacle may be overcome by preparing channels with hydrogels, such as fibrin, suitable to support cell activity and angiogenesis. These hydrogels can be shaped into complex networks by using sacrificial molds, such as gelatin, glass filaments or PDMS[69–71]. Another approach is to directly pattern vascular cells employing cell sheet technology (Figure 9-B), PDMS molds or photopatterning[71].

Given the high degree of vascularization of the skeletal system, microfluidic platforms have been used to develop vascularized bone tissue models. The already published studies present models that aim to address fundamental aspects of bone physiology, namely mechanical strain or hypoxic conditions. Moreover, these platforms allow for co-culture of different cell types seeded in different compartments, while maintaining sprouting potential between them. There are other important aspects to mention besides chip design, such as type of cells used, and materials employed to

support the growth and activity of cells. Concerning the latter, and having the natural composition of bone in mind, researchers have used different matrices ranging from collagen and fibrin hydrogels[72,73], HA-fibrin matrix[74], ectopic bone[75] and ceramic scaffolds[76]. As well as the matrix choice, cell type used is also dependent on the aim of the study. For example, Bersini *et al.*[73], using a collagen type I gel, established a tri-culture between human bone marrow-derived mesenchymal stem cells, human umbilical vein endothelial cells and human breast cancer cells to study the specificity of human breast cancer metastases to bone (Figure 11-D). The purpose of the study was to assemble a bone-specific model to investigate the extravasion of highly metastatic breast cancer cells into a bone biomimetic microenvironment[73]. The inclusion of collagen type I suited this aim, since collagen type I is the main component of the organic fraction of bone ECM. Through this model, the authors were able to: obtain quantitative results regarding extravasion rate and extravased distance by breast cancer cells; identify the role of the CXCR2 (a cancer cell surface receptor) and CXCL5 (a chemokine secreted within bone) molecular pathway in the extravasion process; and show the proliferation and generation of micrometastasis within a biomimetic bone environment[73]. Jeon *et al.*[72] also made use of human umbilical vein endothelial cells (HUVECs) and human bone marrow-derived mesenchymal stem cells (BM-hMSC) to study and optimize the formation of functional microvascular networks, in a 3D fibrin gel. The use of human bone marrow-derived mesenchymal stem cells in these microfluidic bone models is important because of their potential to differentiate into osteoblasts and mural cells, contributing to vessel maturation and stability. The authors compared the microvascular networks generated through HUVEC monoculture and HUVEC-BM-hMSCs co-culture. In addition, they also studied the effect of angiopoietin-1 (Ang-1) and TGF-β1 on the phenotypical transition BM-hMSC to mural cells. It was observed that the optimal condition regarding the formation of functional, perfusable microvascular networks was achieved when co-culturing HUVECs and BM-hMSCs in the presence of VEGF and Ang-1, noticeable by the higher amount of alpha-smooth muscle actin (α-SMA)-indicating the phenotypical transition of the BM-hMSCs- and laminin rich ECM surrounding the microvessels[73]. Other supporting cells may be used, such as lung fibroblasts, known to release angiogenic factors[74]. In the study published by Jusoh *et al.*[74], sprouting from the cell compartment to a bone mimicking fibrin-HA matrix was observed (Figure 11-A). The natural angiogenic properties and growth factors gradually released from fibrin make it a commonly used matrix for microvasculature *in vitro* models[77]. A comparison between fibrin enriched with HA nanoparticles and pure fibrin was set, regarding the angiogenic potential of the matrix.

Fibrin with 0,2% HA has displayed the highest sprouting length and more favorable lumen formation. The authors attributed these effects to higher matrix stiffness when HA is present, as well as adsorption of VEGF to HA nanocrystals, allowing for a controlled release, thus improving bioavailability and efficacy of VEGF delivery[74].

One of the most complete bone vascularized *in* vitro models published so far has included the tetraculture of osteoblasts, osteoclasts, HUVECs and BMSCs (Figure 11-C). Although not assembled within a microfluidic device, Bongio *et al*.[78] established the tetraculture in a collagen/fibrin hydrogel enriched with calcium phosphate nanoparticles (CaPn). In earlier studies from the same group, Bersini *et al*.[79] had already shown this collagen/fibrin hydrogel to be suitable for the co-culture of HUVEC and BMSCs, in which hydrogel composition, medium of culture and cell ratio were optimized. Thus, a vascularized *in vitro* model, at the millimeter scale, was assembled, with use of a bone mimicking substrate to support the formation of 3D vascular networks[80]. In the follow-up study[78], mentioned above, CaPn was introduced within the collagen/fibrin hydrogel to better mimic the bone mineral composition, and osteoblasts and osteoclasts were added to better resemble the cellular microenvironment of bone. It was shown that differentiation towards osteogenic and osteoclastic lineage was enhanced in the presence of constructs enriched with CaPn. Osteogenic activity, by osteoblasts, and resorption activity, by osteoclasts, was also stimulated within these hydrogels. Besides the effect of the presence CaPn within the hydrogels, these responses were exacerbated in tetraculture, as opposed to mono and co-culture conditions (osteoblasts and osteoclasts monocultures, and osteoblast-osteoclast co-cultures). However, the microvascular network formation was reduced in the presence of both osteoblasts and osteoclasts, regardless of hydrogel formulation, possibly due to modification of hydrogel properties, as a consequence of osteoblast matrix deposition, or the high proliferative osteoblasts representing a steric obstacle for ECs[78]. Another study by Middleton *et al*.[81] employed a microfluidic system to assess mechanically regulated osteocyte-osteoclast communication. The proposed strategy allowed for exposure of different cell populations to different levels of fluid

shear stress, and promotion of cell-cell communication between the different channels.

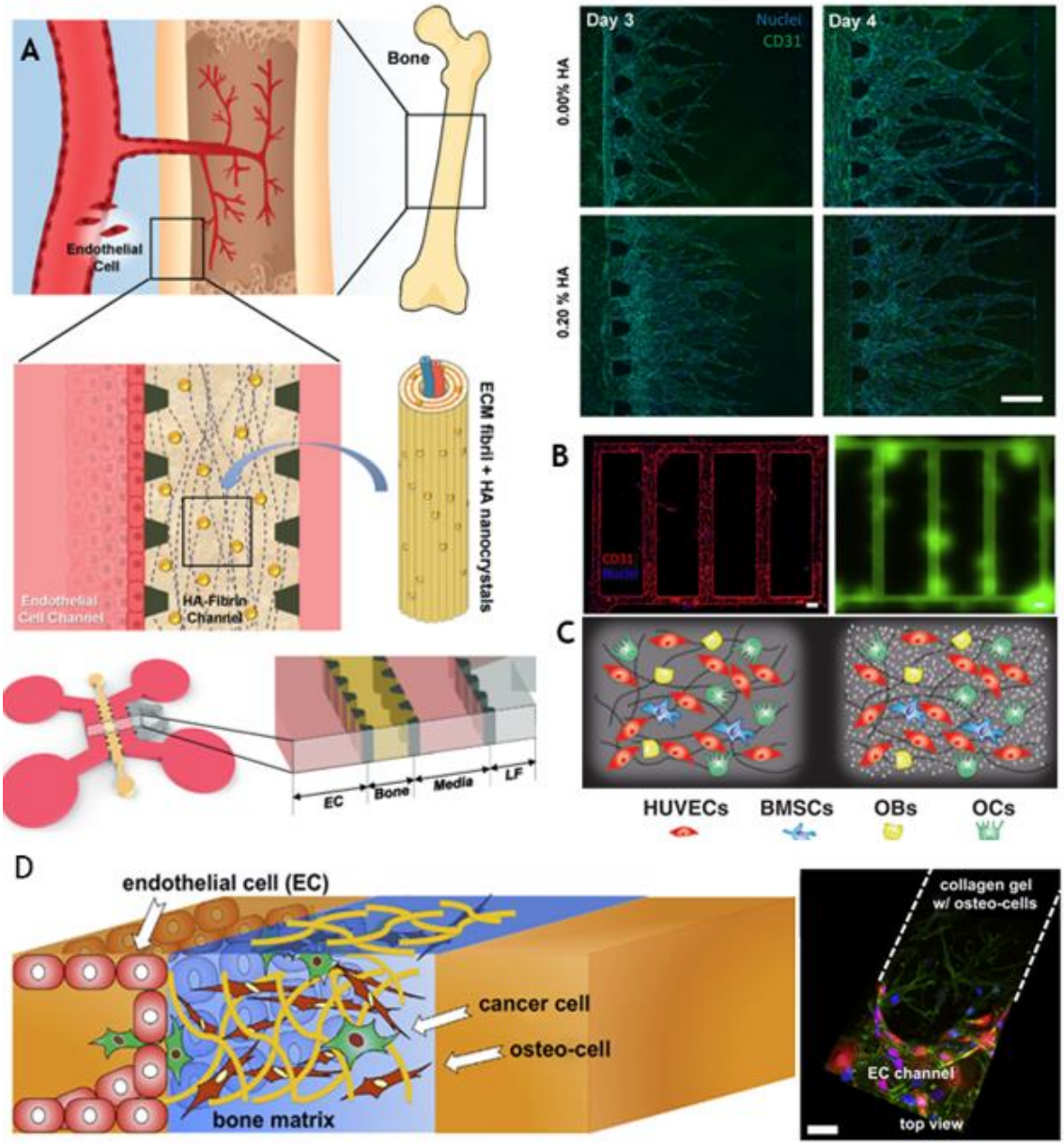

Figure 11- Different strategies and applications of vascularized bone models: A) Schematic representation of bone angiogenesis during development, bone mimicking compartment and microfluidic design; on the right, sprouting from the endothelial cell channel to the fibrin HA-enriched matrix is observed. Adapted from Jusoh *et al.*[74] B) organization of HUVECs in 2D by patterning both cell-adhesive and non-cell-adhesive regions on a 2D surface. By stacking multiple layers, a 3D network is acquired that further remodels during culture. Adapted from Zheng *et al.*[69] C) Schematic representation of HUVECs, BMSCs, osteoblasts (OBs) and osteoclasts (OCs) in plain (left) and enriched CaPn (right) collagen/fibrin hydrogels. Adapted from Bongio *et al.*[78] D) on the left, a schematic representation of a bone metastasis cancer model is displayed; on the right, a top view of the triculture comprised of cancer cells, endothelial cells and osteo-cells microfluidic. Adapted from Bersini *et al.*[73]

Although there is an effort to strongly develop and improve the *in vitro* bone models, the complexity of the bone microenvironment led to the development of modular systems to simplify and successfully understand the interaction between the

different cell types. Still, bone homeostasis is supported and regulated by complex interactions between bone cell populations, vascularization and innervation.

Concerning vascularization, the studies here discussed show that coupling mechanisms between angiogenesis and osteoclastogenesis exist, but the exact effect of ECs on osteoclasts is unclear. Moreover, osteoclasts are reported to have angiogenic potential, but the mechanisms underlying this effect are contradictory and not fully understood. The importance of bone innervation in bone is highlighted through the presence of nerve fibers and the effects of neuropeptides on bone cells, but the mechanisms underlying these effects are not completely known.

Several bone models have been developed, but osteoclasts are often not included as bone cell population. Moreover, these models also do not include any strategy of peripheral innervation. Similarly, models of peripheral innervation have been employed to study the interaction between bone cells and sensory neurons, but vascularization is not considered. Therefore, there is a need to develop *in vitro* models to study the interactions between ECs, osteoclasts, and sensory neurons, and unravel possible mechanisms underlying those interactions, while mimicking the anatomical and physiological characteristics of bone. Microfluidic platforms have emerged as adequate tools to the study of these complex interactions because they allow for the co-culture of different cell populations, under controlled conditions, mimicking complex microenvironments.

This leads us to the goal of this dissertation: to develop a microfluidic *in vitro* model consisting of sensory neurons, ECs and osteoclasts, within a bone mimetic microenvironment.

Aim of the Project

The aim of the present work is to assemble an *in vitro* triculture bone mimicking model consisting of sensory neurons, ECs and osteoclasts. To achieve this goal, several specific aims were raised:

1. Optimization of HUVEC Culture

The first part of the study consists in optimizing HUVECs culture regarding substrate for cell seeding and cell density to promote the formation of microvascular structure.

2. HUVEC Microfluidic Monoculture and Co-culture

After optimizing the above mentioned parameters, HUVECs will be cultured within the microfluidic devices. Co-culture between HUVEC and sensorial neurons will be assembled. Furthermore, endothelial cell marker and neuronal cell marker, as well as cell morphology will be assessed.

3. Triculture Assembling

Sensory neurons, HUVECs and human osteoclasts will be cultured within a microfluidic device designed to mimic the bone microenvironment. The same parameters evaluated in the monoculture and co-culture will be assessed. This triculture model could be a useful *in vitro* model to study cross talk between sensory neurons, ECs and osteoclasts.

4. Potential Angiogenic Effect of Osteoclasts

To unravel the possible paracrine effect of osteoclasts on ECs, a 2D tube formation assay will be performed, in which HUVEC will be treated with human osteoclast conditioned medium.

Chapter II: Materials and Methods

Experimental Overview

In this study, a step-by-step method was followed to assemble a triculture consisting of DRG, HUVECs and human osteoclasts, in a bone biomimetic environment, within a microfluidic platform. Firstly, HUVEC culture conditions amongst different hydrogels were compared. After optimization, HUVEC culture in microfluidic devices was ensued. The second step was assembling a Dorsal Root Ganglia (DRG)-HUVEC co-culture in the microfluidic platform. Finally, a triculture between the above-mentioned cell types was established. In addition, an angiogenic assay was performed to evaluate the paracrine effect of osteoclasts on HUVECs.

1. Cell culture

All animal procedures were approved by the IBMC/INEB ethics committee and by the Portuguese Agency for Animal Welfare (Direção-Geral de Alimentação e Veterinária) in accordance with the EU Directive (2010/63/EU) and Portuguese law (DL113/2013).

1.1. Endothelial Cell Culture

HUVECs were expanded in flasks previously coated with gelatin (Sigma) 0,2% w/v, at 37ºC under a 5% CO_2 humidified atmosphere, in M199 (SIGMA) medium supplemented with 10% v/v inactivated Fetal Bovine Serum (FBS), 1% v/v

Penicillin/Streptomycin (P/S), 90 µg/ml of heparin and 15 µg/ml of Endothelial Cell Growth Supplement (ECGS).

1.2. Sensory Neurons culture

Embryonic DRG were isolated from 16 to 18 days-old murine embryos. These embryos were harvested from pregnant female mice, exposed to isoflurane by inhalation, and kept on ice-cold Hank's balanced salt solution (HBSS, Invitrogen). After spinal cord removal, DRG were successfully obtained by cleaning the meninges and cutting the roots. Until seeding, the ganglia were preserved in cold HBSS.

1.3. Human Osteoclast Culture

Human blood monocytes were obtained from buffy coats, provided by Hospital São João, from female healthy donors. Firstly, the buffy coats were diluted in PBS and delicately layered on top of Ficoll-Paque PLUS (GE Healthcare) solution. Four different layers consisting of plasma, peripheral blood mononuclear cells (PBMC), Ficoll-Paque and red blood cells (RBC) formed as a result of centrifugation at 2000 rpm for 20 minutes and without brake. The PBMC layer was carefully extracted and washed twice in cold PBS. It was after centrifuged at 2000 for 12 minutes twice, with a PBS washing step in between. Following the second centrifugation, PBMC was resuspended in incubation buffer composed of 0,5% Biotin-free BSA (Sigma) in 2 mM EDTA (Invitrogen). The addition of BD IMag™ Magnetic Particles associated with anti-CD14 antibody (BD Biosciences), would allow magnetic separation of CD14 positive monocytes. To that purpose, following a 30 minutes incubation period with the magnetic particles and antibody solution, the suspension was subjected to EasySep magnet for 10 minutes. After discarding the supernatant, cells were washed with incubation buffer. This process was repeated twice. Cell counting was then performed, and $5x10^6$ cells were plated in T-75 flasks. Alpha-minimal essential medium (α-MEM, Gibco) supplemented with 10% FBS, 1% P/S and 25 ng/ml M-CSF (R&D Systems) was added to each flask. Cells were incubated at 37ºC with 5% CO_2. At day 2 after isolation, medium was collected and centrifuged. The pellet was resuspended in α-MEM supplemented with 10% FBS, 1% P/S, 25ng/ml M-CSF and 25 ng/ml RANKL and placed into the culture flask. At days 5 and 7, medium was replaced.

2. Extracellular matrix optimization for Endothelial Cell culture

2.1. 2D Tube Formation Assay

Prior to cell harvesting, three different hydrogels were prepared: Matrigel®, fibrin and Collagen/Fibrin (Col/Fib) hydrogels.

Fibrin hydrogels were prepared by mixing equal volumes of a solution of fibrinogen (Sigma-Aldrich) and a thrombin solution. The solution containing thrombin (Sigma-Aldrich) at 2 U/mL also included 2,5 mM $CaCl_2$ (Sigma-Aldrich) and 10 µg/mL of aprotinin (Sigma-Aldrich), dissolved in tris-buffered saline (TBS). The final concentration of fibrinogen upon mixing with thrombin solution was 6 mg/mL.

Collagen/Fibrinogen solutions were prepared by mixing by mixing Collagen type I and fibrinogen at a mass ratio of 40:60 (final concentration 1,875 mg/mL). Preparation of Collagen type I was performed according to manufacturer's instructions (CORNING®), to a concentration of 3,0 mg/mL. Fibrinogen was previously diluted in TBS to a concentration of 4,5 mg/mL. Thrombin solution was prepared by diluting it to 4 U/mL in M199 medium. Collagen/Fg and thrombin solution were mixed 1:1, forming a Col/Fib hydrogel.

Matrigel® (CORNING®) was kept on ice after thawing overnight (O/N) at 4ºC. It was then mixed 1:1 with M199 medium. All Eppendorf's and pipette intended to manipulate Matrigel® were kept at 4ºC.

Prior to cell seeding, Matrigel®, fibrin and Col/Fib hydrogels were plated on µ-Slide Angiogenesis® (Ibidi) and left to polymerize for 60, 30 and 30 minutes respectively, at 37ºC and 5% CO_2.

Upon reaching 80-90 % confluence, HUVECs were washed with PBS and incubated with 0,25% trypsin (Sigma) for 5 minutes at 37ºC and 5% CO_2. Trypsin effect was neutralized through the addition of FBS containing medium in equal proportion. Cells were then centrifuged at 1100 rpm for 5 minutes and resuspended in endothelial cell growth medium-2 (EGM-2, Lonza) with 15 µg/mL ECGS and seeded on top of the hydrogels at a final density of $8x10^4$ cells/cm^2 (Figure 12). Culture was maintained for 48 hours. At the 24-hour time point, cells were photographed using an inverted fluorescence microscope (AxioVert 200, Zeiss) connected to a digital camera (AxioCam

MRm, Zeiss) to observe the formation of tubular like structures. At 48 hours staining for F-actin and nuclei was performed.

Figure 12-µ-Slide Angiogenesis® :2D cell culture: cells are seeded on top of a hydrogel. Adapted from µ-Slide Angiogenesis® Sheet.

2.1.1. Immunocytochemistry

Medium from each well was collected and cells were washed with PBS. Then, fixation was performed with paraformaldehyde (PFA, Merck) 4 wt.% in PBS for 10 minutes. After removing PFA, cells were washed with PBS. A permeabilization step was performed, in which cells were incubated with 0,1% v/v TritonX-100 (Sigma) for 5 minutes. Cells were then incubated with a blocking solution, consisting of PBS with 1% Bovine Serum Albumin (BSA) (Sigma-Aldrich), for 30 minutes.

For further microscopical observation, filamentous action of the cells 'cytoskeleton was bond to green-fluorescent phalloidin (Alexa Fluor 488; Invitrogen) in a 1:100 dilution for 60 minutes, in the dark, at room temperature (RT). The nuclei were stained with propidium iodide (PI, Sigma) in a dilution of 1:3000, for 5 minutes at RT. The results were examined under a CLSM Leica SP5 AOBS SE equipped with LCS 2.61 software (Leica Microsystems, Inc.).

2.2. 3D Endothelial Cell Culture

2.2.1. Cell Seeding

Hydrogels were prepared as described above. Cells were harvested and after centrifugation, resuspended in M199 Complete medium (10% FBS, 1% P/S and 90 µg/mL heparin). Equal volumes of cell suspension were collected for the fibrin and Col/Fib conditions, in order to achieve a final cell density of $10x10^6$ cells/mL or $20x10^6$ cells/mL. Cells were then centrifuged at 1200 rpm for 5 minutes. After discarding the supernatant, cells destined for the fibrin gel were resuspended in the thrombin solution and homogeneously mixed 1:1 with the fibrinogen solution (Figure 13). For the Col/Fib hydrogel, the cells were resuspended within the thrombin solution and

mixed 1:1 with the collagen/fibrinogen solution. Both hydrogel types polymerized for 30 minutes, at 37º and 5% CO_2. After polymerization, EGM-2 medium supplemented with 15 µg/mL ECGS was added and cells were incubated at 37ºC and 5% CO_2. A positive control (2D Matrigel® setup) was prepared for a final density of $4x10^4$ cells/cm^2 per well. Matrigel® was mixed 1:1 with M199 medium and left to polymerize for 60 minutes, at 37ºC and 5% CO_2. After gel polymerization, HUVECs were directly resuspended in EGM-2 and seeded on top of the Matrigel® layer.

Culture was held for 36 hours. Medium was replaced for all conditions after 24 hours of culture. At 36 hours, viability assay was performed. Afterwards, cells were fixed and stained for nuclei and F-actin, as described above.

Regarding the highest cell density, metabolic assay and morphology were evaluated at 24, 48, 72 and 96 hours. Medium was replenished every 24 hours.

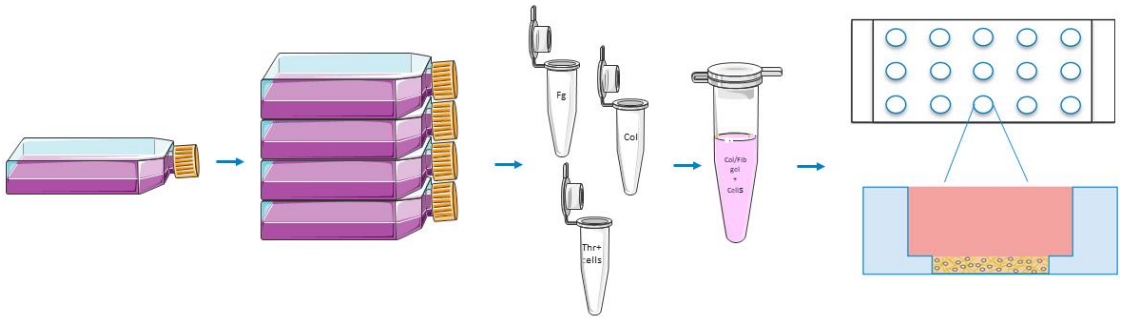

Figure 13-Schematic representation of the experimental procedure for the cell seeding in 3D cell culture, using µ-Slide Angiogenesis®; Adapted from µ-Slide Angiogenesis® Sheet.

2.2.1.1. Viability Assay

Cells were then washed with PBS and incubated with Calcein AM (Invitrogen) diluted 1:10000 in PBS, in the dark for 20 minutes at 37ºC and 5% CO_2. Calcein solution was then discarded and PI was added at 1:3000 dilution in PBS for 10 minutes, in the dark. Cells were after washed and incubated with PBS.

For the cell density of $20x10^6$ cells/mL, dilution of each reagent was adjusted to 1:250, in the case of Calcein, and 1:2000 in the case of PI. The results were examined under a CLSM Leica SP5 AOBS SE equipped with LCS 2.61 software or Leica SP2AOBS equipped with LCS 2.61 software.

2.2.1.2. Cell Morphology

Cells were washed with PBS and fixed with PFA 4 wt.% in PBS for 10 minutes. After removing PFA, cells were washed with PBS. Cells were then incubated with a

blocking solution, consisting of PBS with 1% BSA and 0,2% v/v TritonX, for both permeabilization and prevent antibody unspecific binding.

For further microscopical observation, filamentous action of the cells'cytoskeleton was bond to green-fluorescent phalloidin (Alexa Fluor 488; Invitrogen) in a 1:100 dilution for 60 minutes, in the dark, at room temperature (RT). The nuclei were stained with 6-diamidino-2-phenylindole dihydrochloride (DAPI, Sigma) in a dilution of 1:10000, for 5 minutes at RT. The results were examined under a CLSM Leica SP5 AOBS SE equipped with LCS 2.61 software (Leica Microsystems, Inc.).

2.2.1.3. Metabolic Assay

Metabolic activity was assessed for the condition of highest cell density, at 24, 48, 72 and 96 hours through resazurin assay (Sigma). Resazurin was added to EGM-2 at 10% (v/v) supplemented with 15 µg/mL ECGS. Cells were incubated with the prepared Resazurin containing EGM-2 for 4 hours at 37ºC and 5% CO2, in the dark. Fluorescence was then read with an excitation at 530 nm through a SynergyTM Mx Microplate Reader (BioTek).

3. Microfluidic Cultures

3.1. Preparation of Microfluidic Devices

3.1.1. Microfluidic Fabrication

Microfluidic devices were fabricated through soft lithography, as described by Park *et al.*[64] (Figure 14). Prior to the microfluidic assemble, the PDMS was punctured with a 2mm punch to allow DRG culture. The PDMS was also wrapped in tape to remove any debris that might interfere with cell culture. Afterwards, it was cleaned with ethanol 70% and left to dry O/N, in sterile conditions.

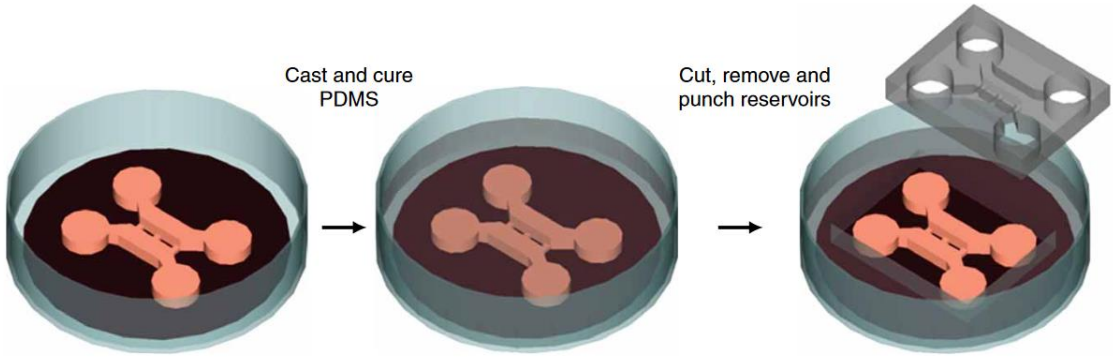

Figure 14- Schematic representation of microfluidic platform fabrication by soft lithography. Adapted from Park *et al*.[64].

3.1.2. Coverslip Preparation

Glass coverslips were incubated with nitric acid (65%) O/N at RT, under mild agitation. The following day, coverslips were rinsed thoroughly to achieve neutral pH. Washing steps with deionized water (d-H_2O) were repeated. Afterwards, in sterile environment, the coverslips were rinsed with alcohol from 5 to 10 minutes and left to dry O/N. The coverslips were then stored in sterile petri dishes until further use.

3.1.3. Microfluidic Assembling

With the exception of the triculture, microfluidic devices were sealed by gently, but firmly, pressing the PDMS against the glass coverslip.

In the case of the triculture, the sealing was performed after oxygen plasma treatment. Both glass cover slips and PDMS device were subjects of plasma treatment. The microfluidic was then assembled by pressing the PDMS against the coverslip.

3.2. HUVECs monoculture

After assembling the microfluidic devices (Figure 15), these were kept on 4ºC until cell seeding. Col/Fib and Matrigel® substrates were used. Preparation of the hydrogels was ensued as described in point 2.1. To ensure 3D cell culture within both Col/Fib and Matrigel® substrates, cell seeding was followed as detailed previously, in point 2.2.2. Medium was replaced every 24 hours for EGM-2 supplemented with 15 µg/mL ECGS. Cultures were held for 24, 48 and 72 hours. Morphology and CD31 expression was assessed throughout the different timepoints.

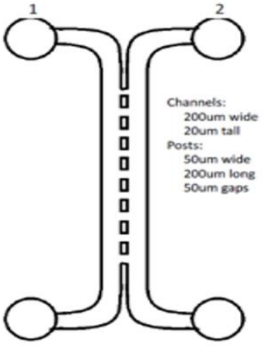

Figure 15- Microfluidic devices employed for HUVECs monoculture.

3.2.1. Cell Morphology and CD31 Expression

At 24, 48, and 72 hours, fixation, permeabilization and blocking of cultures were performed as described previously, in point 2.2.2.3. Cells were then incubated with anti-CD31 primary antibody (Santacruz Biotechnology) diluted 1:100 in PBS with 1% BSA and 0,2% v/v TritonX-100, O/N at 4ºC. Next, incubation with secondary antibody Alexa Fluor 568 (Invitrogen) diluted 1:1000 in PBS, in the dark. Afterwards, cells were washed with PBS and incubation with DAPI followed for 5 minutes, at RT, in the dark. Cell were then washed with PBS. The results were examined under a CLSM Leica SP5 AOBS SE equipped with LCS 2.61 software or CLSM; Leica SP2AOBS.

3.3. DRG-HUVEC Co-culture

After HUVECs culture optimization within the microfluidic device (Figure 16), a DRG-HUVEC co-culture was established.

Prior to cell seeding, the channels of the microfluidic devices were coated with Poly-D-lysine (PDL, Sigma) at 0,1 mg/mL O/N. PDL was then washed three times with autoclaved d-H_2O and followed by an additional coating step with Laminin solution 5 µg/mL in neurobasal medium (Gibco).

After microfluidic preparation was completed, HUVECs were firstly seeded in the microfluidic device. Cell detachment and hydrogel preparation were proceeded was described previously. HUVECs were cultured within Matrigel®, at a cell density of $20x10^6$ cells/mL. Matrigel® was allowed to polymerize for 30 minutes at 37ºC and 5% CO_2. EGM-2 supplemented with 15 µg/mL ECGS was then added to each well of the axonal side of the microfluidic devices. EGM-2 was replenished every 24 hours.

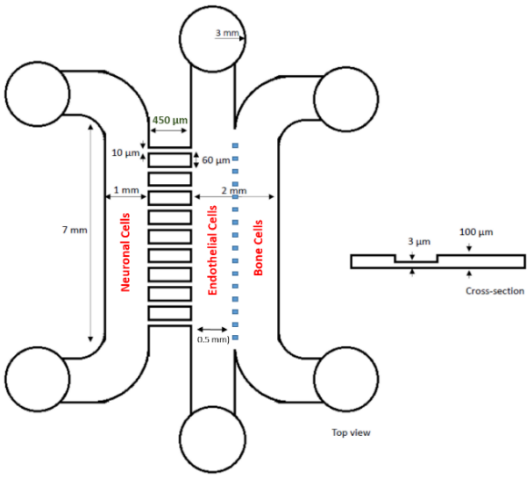

Figure 16- Microfluidic platforms used for the establishment of the sensory neurons-endothelial cells-human osteoclasts triculture. DRG was cultured on the somal side (left), and endothelial cells and osteoclasts were cultured on the axonal side (right).

Soon after DRG isolation, previously described, the ganglion was added to the somal compartment. Neurobasal medium supplemented with 2% v/v B-27 Serum-Free Supplement® (B-27, Invitrogen), 60 µM 5-fluoro-2'- deoxyuridine (FDU, Sigma-Aldrich), 25 mM glucose (Sigma-Aldrich), 1 mM pyruvate (Sigma- Aldrich), 50 ng/mL 7S Nerve Growth Factor (NGF, Calbiochem, Merck Millipore), 2 mM glutamine (BioWittacker, Lonza, Basel, Switzerland) and 1% P/S was also added to each well of the somal compartment.

The co-culture was maintained for 48 hours. Cell morphology, CD31 expression and neuronal specific marker ß-III tubulin were assessed.

3.3.1. Cell morphology, CD31 and ß-III tubulin Expression

Both the embryonic DRG and HUVECs were fixed with 4% of PFA in PBS with 4% sucrose, for 10 minutes at RT. Following fixation, cells were incubated with blocking solution for 30 minutes. Cells were then incubated O/N, at 4ºC, with a blocking solution containing both primary antibodies for CD31 (Santacruz Biotechnology), diluted 1:100, and ß-III tubulin (Promega), diluted 1:2000. Afterwards cells were washed with PBS and incubated with secondary antibodies, Alexa Fluor 488 and 568 (Invitrogen), for 60 minutes at RT. Subsequently, co-culture was incubated with Alexa Fluor phalloidin 647, diluted in PBS 1:40, O/N at 4ºC. After washing with PBS, incubation with Hoechst 33342 (Life Tech), diluted 1:10000 in PBS, was performed for 5 minutes at RT. Cells were then incubated with PBS. Images were captured with a confocal laser scanning microscope (CLSM) Leica SP2 AOBS SE equipped with LCS 2.61 software (Leica Microsystems, Wetzlar, Germany).

3.4. Sensory Neurons-Endothelial Cells-Human osteoclasts Triculture

Prior to cell seeding, plasma sealed microfluidic devices were incubated with ethanol 70% for 5 minutes. After incubation, ethanol was thoroughly aspirated, using a suction system, and microfluidic chambers were washed with autoclaved d-H_2O three times. PDL solution at 0,1 mg/mL was added to each channel and incubated O/N at 37ºC and 5% CO_2. Following incubation, the channels were once again washed with autoclaved d-H_2O. Afterwards, the microfluidic devices were incubated with M199 complete medium for protein adsorption. Subsequently, laminin 5 µg/mL in neurobasal medium coating was applied until cells were seeded within the devices.

The first cell type to be seeded within the microfluidic devices (Figure 16) were HUVECs. Cell detachment and hydrogel preparation were proceeded was described previously. HUVECs were cultured within Matrigel® and Col/Fib hydrogels, at a cell density of $20x10^6$ cells/mL. Hydrogels were allowed to polymerize for 30 minutes at 37ºC and 5% CO_2. EGM-2 supplemented with 15 µg/mL ECGS was then added to every well until further cells were cultured.

DRG were cultured in the somal compartment in supplemented neurobasal complete medium.

Osteoclasts were isolated as described previously (section 1.3). At day 9 of differentiation, accutase (Gibco) was added to each flask and incubated for 10 minutes, a 37ºC and 5% CO_2. α-MEM containing FBS was added to each flask and cells were detached using a cell scrapper. After centrifugation for 5 minutes at 1500 rpm, cells were count and later seeded within the microfluidic devices at $5x10^4$ cells per microfluidic channel. Osteoclasts were left to adhere for two hours. Afterwards α-MEM supplemented with 10% FBS, 1% P/S, 25ng/ml M-CSF and 25 ng/ml RANKL was added to the osteoclast compartment of each device.

The triculture was held for 96 hours, incubated at 37ºC and 5% CO_2. EGM-2 supplemented with 15 µg/mL ECGS was replaced every 24 hours. Neurobasal complete medium and α-MEM containing cytokines were added to their respective compartments to avoid evaporation. After 96 hours the triculture was fixed and immunocytochemistry for cytoskeleton, CD31 expression and ß-III tubulin marker was performed as previously described.

4. Angiogenic Potential of Osteoclasts

4.1.1. Osteoclast Culture

Osteoclasts were isolated and seeded in a 96 well plate, at a density of $5x10^4$ cell/well, within the following conditions:

a) α-MEM with 10% FBS;
b) α-MEM with 0,5% FBS;
c) α-MEM with 10% FBS, on top of bone slices.

Two control conditions, with no added cells, namely α-MEM with 10% FBS, and α-MEM supplemented with 0,5% FBS were also incubated for 3 days at 37ºC and 5% CO_2. All condition contained 1% P/S, 25ng/ml M-CSF and 25 ng/ml RANKL. Afterwards, medium of each condition was collected centrifuged at 1200 rpm for 5 minutes, 4 ºC and stored at -80ºC. Osteoclasts were then fixed with a 4% PFA and 4% Sucrose solution and cell morphology evaluated as previously mentioned.

4.1.2. 2D Tube Formation

Corning® BioCoat™ Matrigel® Matrix Thin-Layer 96 well plate was incubated with M199 for 60 minutes, at 37ºC. Osteoclast conditioned medium collected previously was thawed on ice until cell seeding. HUVECs were detached from cell culture flaks as previously detailed. M199 medium was collected from the 96 well plate and discarded. Cells were carefully resuspended in medium corresponding to each experimental condition and seed to each well at $6,25x10^4$ cells/cm^2 (Figure 17). After cell seeding, the 96 well plate was incubated at 37ºC, under humidified atmosphere with 5%CO_2. Cells were imaged at 0,3,6,9 and 24 hours using an INCell Analyzer 2000 equipped with IN Cell Investigator software (GE Healthcare, Little Chalfont, UK).

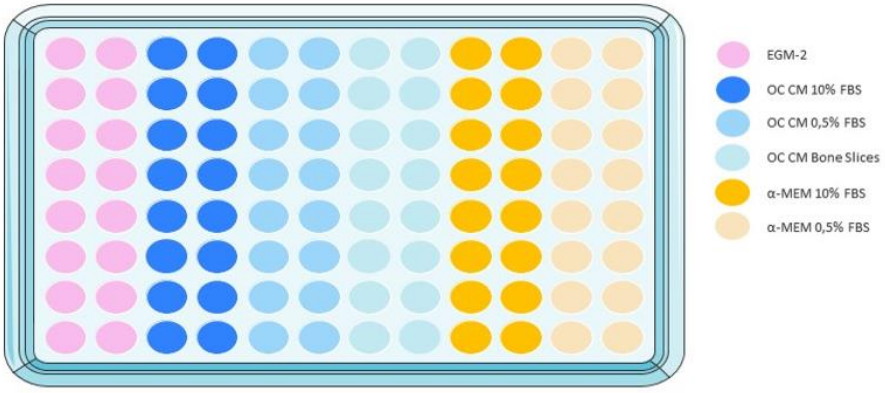

Figure 17-Experimental design to assess the angiogenic potential of osteoclasts.

This page was intentionally left in blank

Chapter III: Results and Discussion

Extracellular matrix substrate for endothelial cells culture

Optimization of cell culture conditions, namely cell density and time of culture, was performed using three different substrates. Matrigel®, a commercially available basement membrane extract, was used as positive control, since it is widely described for the culture and maturation of ECs[82]. Fibrin and collagen/fibrin (Col/Fib) hydrogels were used as potential substrates to sustain endothelial cell culture. Fibrin hydrogels have been used in a wide number of angiogenic and vasculogenic *in vitro* models. Fibrin is involved in the process of wound healing, as a temporary matrix, and stimulates the production of extracellular matrix proteins showing natural angiogenic potential[77]. On the other hand, the choosing of the Col/Fib hydrogel was based on its convenient properties for tissue engineering applications, namely availability, easiness of use, biocompatibility and activity. Importantly, collagen I is the main component of the organic fraction of bone matrix, playing an important structural role. Paired with the above-mentioned fibrin properties, a hydrogel composed of a mixture of these components constitutes a suitable candidate for the assemble of vascularized bone models. Moreover, this matrix has been used previously in 3D organotypic cultures that aimed to replicate the process of bone remodeling[78,83].

2D and 3D cultures of ECs were performed, and cell viability, metabolic activity and morphology were assessed. These studies were conducted using µ-Slide Angiogenesis® that allow both 2D and 3D cell culture, depending on the desired condition. Tube formation assays have been used extensively in angiogenesis research to assess the angiogenic potential, either pro or anti, of different molecules[84]. In this

context, it was used to assess the angiogenic potential of the different substrates to be used for endothelial cell culture. The type of ECs used was human umbilical vein endothelial cells (HUVECs). HUVECs have been chosen because they are the most well characterized type of ECs, are easy to obtain and to handle. Furthermore, they represent the most used endothelial cell type in research regarding biomaterial-endothelium interactions[85]. However, it is important to mention that other endothelial cell types may be used in studies of angiogenesis and vasculogenesis.

1. 2D Tube Formation Assay

To perform 2D tube formation assay, cells were seeded on top of three different substrates (Matrigel®, Col/Fib and fibrin) at a density of $8x10^4$ cells/cm^2, for 48 hours. For the 2D cultures it was observed that ECs organized into well-defined tubular like structures when seeded on top of Matrigel® and maintained up until 48 hours of culture.

Regarding the Col/Fib, at 24 hours, cells started to organize in round structures, possibly indicating the early arrangement of tubular like structures (Figure 18, white arrows). The fibrin gel condition, for the same time point, did not display the same structures, nor in the same stage of development, and the cells' morphology resembles the appearance of expanding cells in the absence of hydrogel. At the 48 hours timepoint, the differences between these two conditions remained visible, with the cells seeded on top of the Col/Fib gel displaying the same structures observed before, but at a higher number. Still, at 48 hours of culture, it was not possible to quantify the tubular like structures for either Col/Fib or fibrin gels (Figure 19, white arrows) since quantifications methods usually measure different parameters such as

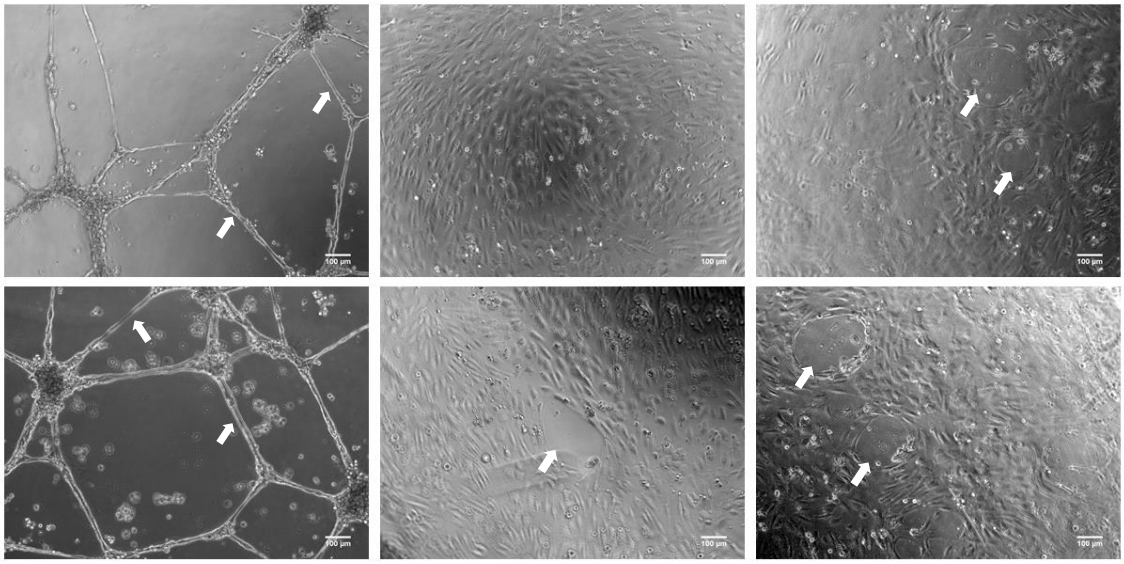

Figure 18-Tube formation assay at 24 hours: Matrigel®, Fibrin hydrogel and Collagen/Fibrin hydrogel, respectively (from left to right). White arrows highlight tubular like structures.

number of tubes; number of loops; number of branch nodes and length of tubes[86]. Herein, the Matrigel® condition displayed mature tubular-like structures. Nevertheless, these results suggest the Col/Fib hydrogel to be a suitable matrix for endothelial cell culture. Other studies have reported rapid formation of tubular structures in fibrin and collagen matrices (from 5 to 8 hours)[87,88], but longer assays have also been reported[41].

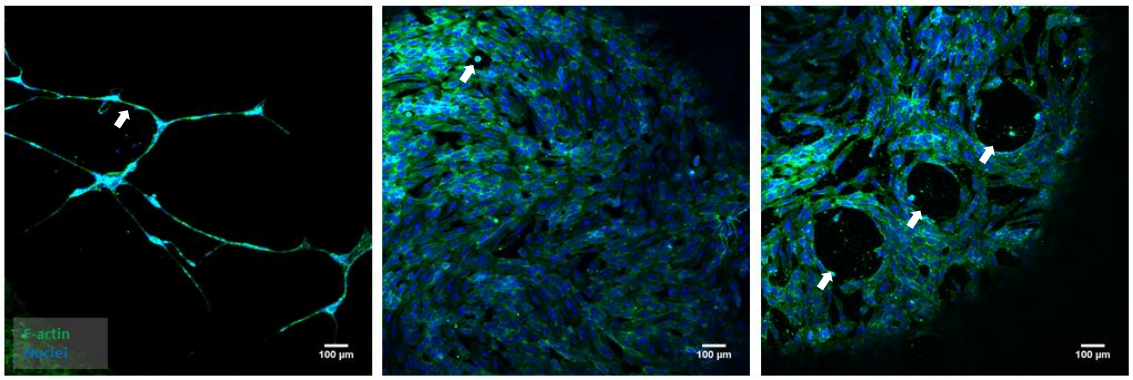

Figure 19-Tube formation assay at 48 hours: Matrigel®, Fibrin hydrogel, and Collagen/Fibrin hydrogel respectively (from left to right). White arrows highlight tubular like structures. Staining: green, F-actin; blue, nuclei.

2. 3D Endothelial Cell Culture

The 3D cultures of ECs were performed testing four different cell densities: 2,3 million cells/mL; 4,67 million cells/mL; 10 million cells/mL; and 20 million cells/mL. In this study, the lower cell density tested proved to be insufficient to assure cell viability, although it has been used successfully in a tetra-culture model[78] (comprising osteoblasts, osteoclasts, ECs and bone marrow mesenchymal stem cells). The same results were obtained for the cell density of 4,67 million cells/mL. In both cases, cells did not remain viable shortly after seeded, possibly due to lack of cell-cell contact (data not shown). Both 10 $x10^6$ and 20 $x10^6$ cells/mL were tested afterwards. Both cell densities sustained cell viability and proliferation, regardless of the hydrogel formulation. However, when compared to the highest density tested, the cells seeded at $10x10^6$ cells/mL present a rounder morphology, observable through F-actin and nuclei staining (Figure 20, white arrows). The cells seeded at $20x10^6$ cells/mL were

more spread across the hydrogels and primitive tubular like structures were observed (Figure 21, white arrows).

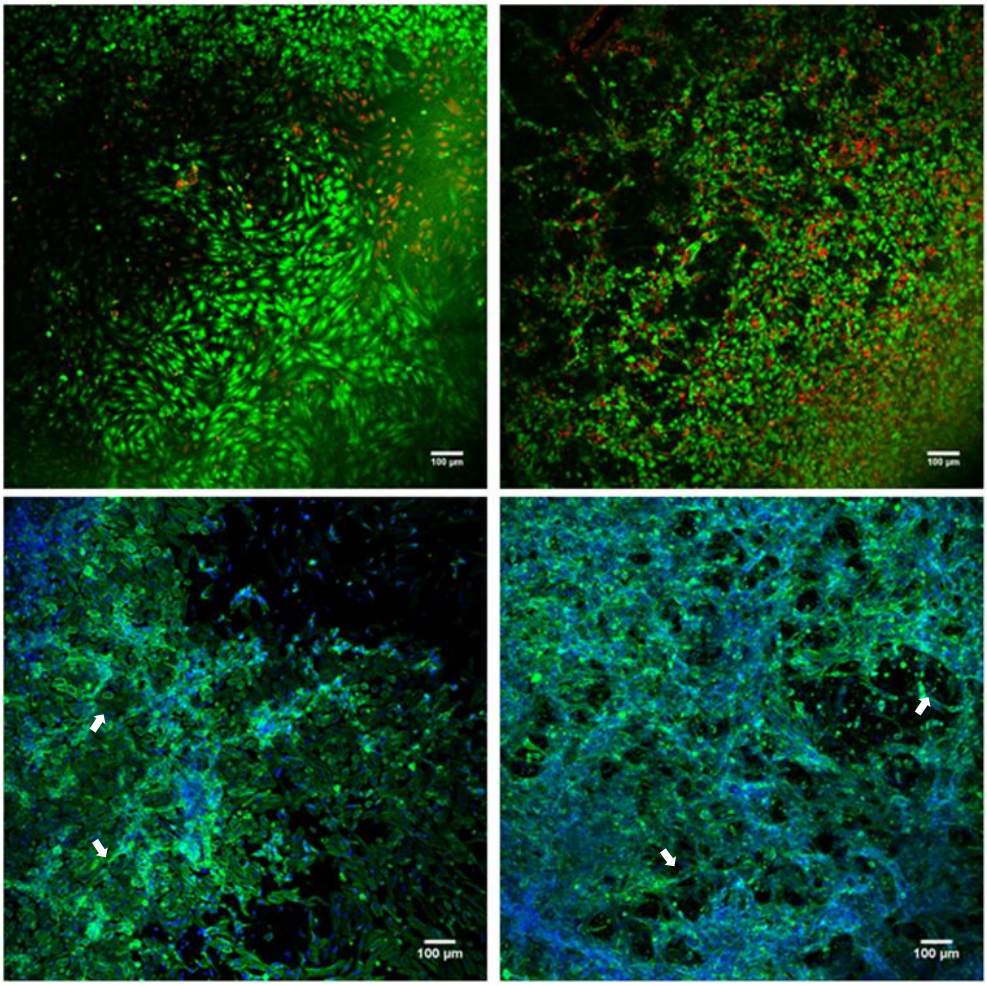

Figure 20- HUVECs seeded within fibrin (left) and Collagen/Fibrin hydrogels (right), at 36 hours of culture. Top images represent Live/Dead assay; bottom images represent nuclei (blue) and F-actin staining (green). White arrows highlight tubular like structures.

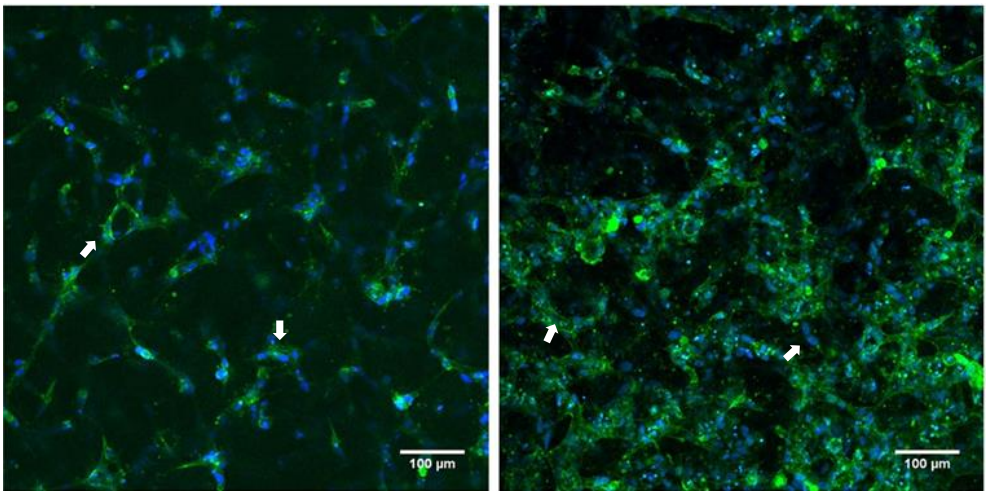

Figure 21- HUVECs seeded on fibrin and Collagen/Fibrin hydrogels, at 48 hours of culture (from left to right). Compared with Figure 20, gels present more mature tubular like structures. White arrows highlight tubular like structures. Staining: green, F-actin; blue, nuclei.

Given the above-mentioned observations, the selected cell density for the following experiments was $20x10^6$ cells/mL. Within this condition, to evaluate the performance of the different hydrogels for the 3D culture metabolic assay, viability assay, as well as staining for cell morphology were performed. While morphology and metabolic activity of cells were assessed at 24, 48, 72 and 96 hours, viability assay was conducted at 24 and 96 hours.

Resazurin, a blue non-fluorescent dye, is broadly used as an indicator of cell viability, proliferation and activity. In metabolic active cells, resazurin is reduced to a pink, high fluorescent resofurin, mostly by mitochondrial reductases. The level of reduction can then be quantified[89]. In the graph shown (Figure 22), higher fluorescence values correlate to higher metabolic activity. Throughout the 96 hours of culture, the fluorescence values remained similar between the different timepoints. Importantly, comparing the different hydrogels for a given timepoint, no value discrepancies were observed. These data imply that the cells presented similar metabolic activity across the three hydrogels, throughout the 96 hours of culture. Through the viability assay, it was possible to observe that at the 24 hours timepoint there was a low amount of dead cells across all three gel types (Figure 23). After 96 hours of culture, the amount of living cells remained visibly higher for all conditions, even though the number of dead cells was more pronounced in the Col/Fib hydrogel, possibly due to a slower degradation of the hydrogel (not assessed) keeping the cells in a more compact structure (Figure 23)[90].

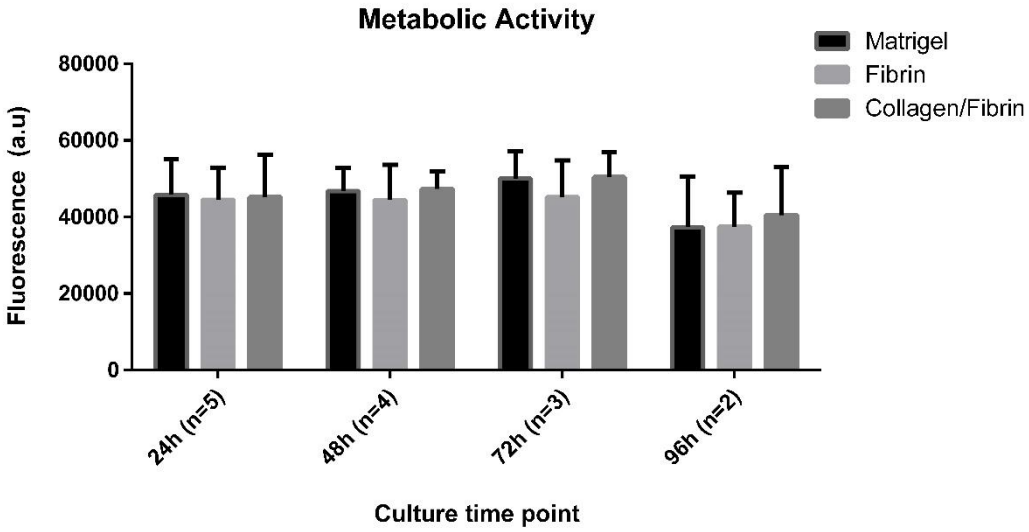

Figure 22- Quantification of metabolic activity through Resazurin assay at 24, 48, 72 and 96 hours. Bars represent Mean ± Standard Deviation values.

In this assay, living cells identification is related to esterase activity, responsible for the conversion of Calcein AM into Calcein and consequent green fluorescence. On the other hand, the identification of dead cells is related with the binding of propidium iodide to DNA of dead cells, which is unable to cross the membrane of living cells.

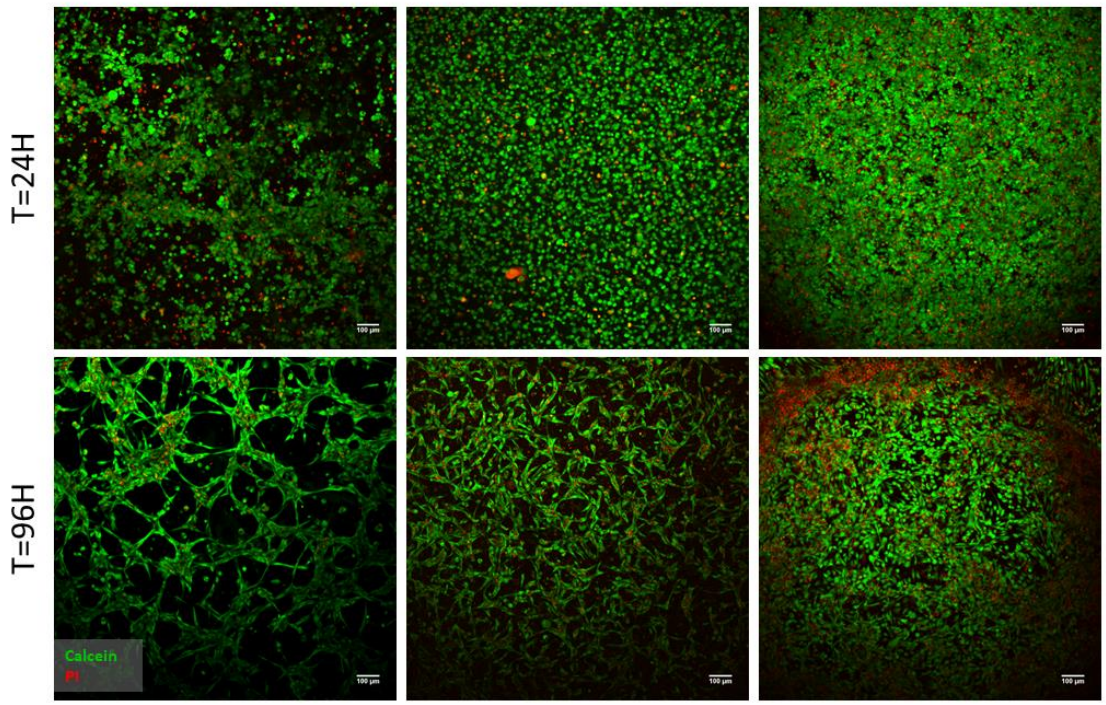

Figure 23- Viability assay of Endothelial Cells seeded, at a density of 20 million cells/mL, in Matrigel, Fibrin and Collagen/Fibrin hydrogels, respectively (from left to right), at 24 (top) and 96 (bottom) hours of culture. Staining: green, live cells; red, dead cells.

Regarding cell morphology, as expected, Matrigel® consistently displayed faster and more mature development of tubular structures and cellular networks, (Figure 24, Figure 25, white arrows). In the both remaining conditions, the cells also organized into tubular structures, but at a slower rate. Differences can be observed between Col/Fib and fibrin hydrogels, regarding maturation of the tubular structures. The fibrin condition displayed more elongated structures, closer resembling the morphology found within the Matrigel® condition. Tubular structures were also present in the Col/Fib condition but at an earlier stage of maturation. Moreover, cells seeded within the Col/Fib gel remained more densely packed, opposing to both fibrin and Matrigel® conditions. ECs produce a laminin-rich basement membrane matrix that provides organizational stability to other cells. During angiogenesis, this matrix is remodelled with the help of matrix metalloproteinases. This dynamic ECM regulates events such as migration, invasion, survival and cell proliferation[91], allowing for appearance of the same networks and tubular structures, but at a slower rate and consequently present a lower maturation.

Another aspect worthy of consideration is matrix stiffness. Other authors have reported that matrix stiffness regulates the degree of vessel-like structure formation, stating that vasculogenesis is favoured in softer matrices [92,93]. Moreover, the authors compared the stiffness of both this Col/Fib hydrogel formulation and fibrin hydrogel, observing that Col/Fib matrices represent stiffer hydrogels[92]. Other studies have reported that capillary networks formed in softer gels often are thinner and denser, compared to those of stiffer hydrogels[93]. Also, capillary growth rates are usually faster in fibrin gels, when compared to collagen[92]. These observations might explain the differences here displayed between the vascular networks present in our experiments.

The formation of vascular networks here observed, has also been studied in previous reports, in which comparisons between Col/Fib and Fibrin gels were established, as well as optimization of the former [78-80].However, in those studies, the cultures were held for longer periods of time, up until ten days or more, allowing for better cell organization and maturation of tubular like structures. In this case, the 96 hours of culture time did not seem enough to achieve similar levels of cellular organization and vascular-like networks. Bongio *et al.*[78] also co-cultured HUVECs and bone marrow mesenchymal stem cells (BMSCs). The inclusion of mesenchymal stem cells BMSCs, acting as perivascular cells, proved to support endothelial cell-mediated neovessel formation and maturation by secreting pro-angiogenic cytokines and controlling neovessel permeability[80]. Within this collagen/fibrin hydrogel, cells remained viable throughout a ten day culture, while retaining their specific functions[78].

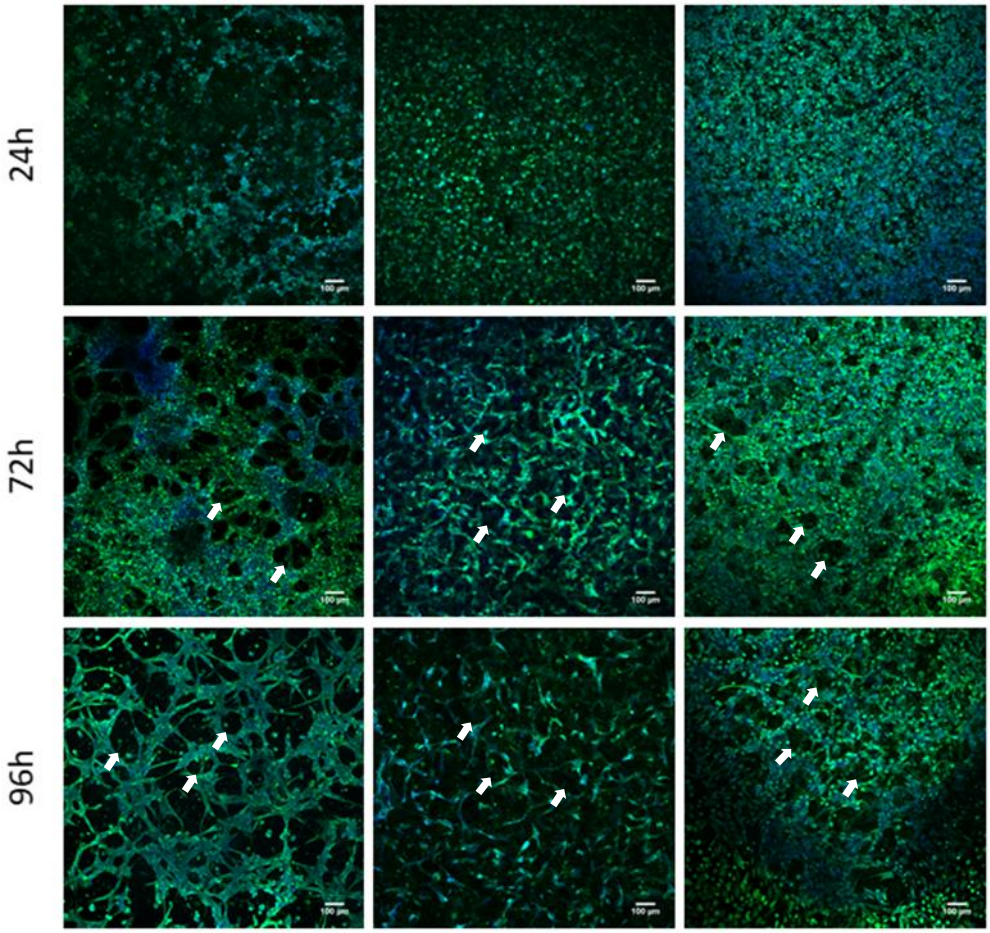

Figure 24 -HUVECs 3D culture in different ECM substrates: (left to right) Matrigel®; Fibrin; Collagen/Fibrin, at 24, 72 and 96h. Matrigel® presents the most mature tubular like structures, followed by fibrin and Collagen/Fibrin. White arrows highlight tubular like structures. Staining: green, F-actin; blue, nuclei.

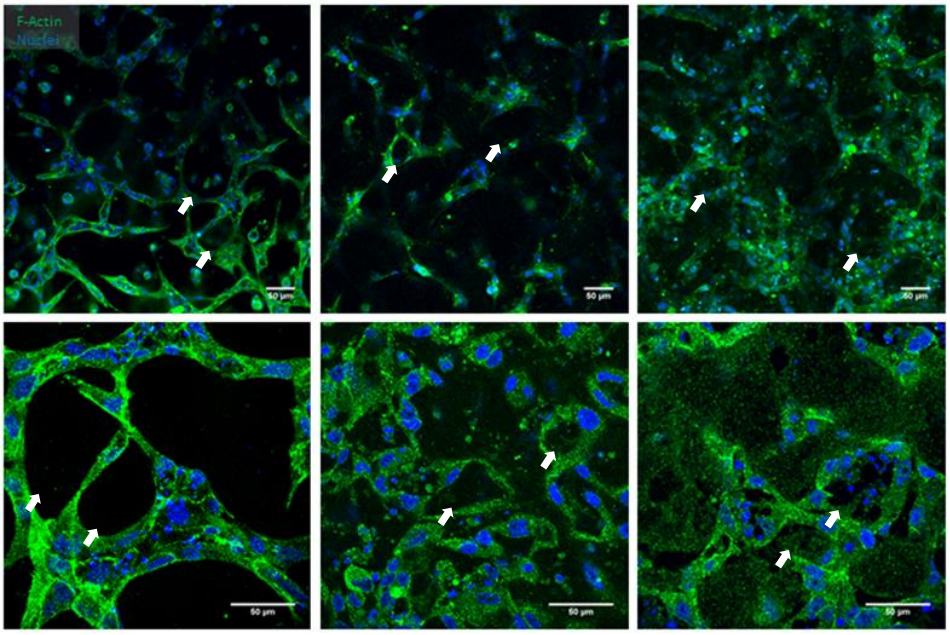

Figure 25 -Detailed representation of HUVECs seeded on Matrigel®, fibrin and Collagen/Fibrin hydrogels, at 48 hours of culture (from left to right). White arrows highlight tubular like structures. Staining: green, F-actin; blue, nuclei.

The experiments performed in this section showed that during 96 hours of culture, there was an increase in cellular organization and morphological complexity towards the formation of vascular structures. All three hydrogels were able to sustain cell viability and activity. The Col/Fib gel showed to be a suitable alternative to both Matrigel® and fibrin as a matrix with angiogenic potential for HUVEC culture envisioning the addition of bone cells into the system. Consequently, both Matrigel® and Col/Fib hydrogels were chosen to sustain HUVECs culture at 20 million cell/ml cell density, for 96 hours, in the following specific aims of establishing the microfluidic-based bone model. Furthermore, the employment of a collagen-based hydrogel better suits the purpose of assembling a vascularized bone model, given that collagen type I is the main constituent of the organic fraction of bone ECM.

Optimization of endothelial cells culture in microfluidic platform

1. Matrigel and Col/Fib (results of cell morphology, time of culture and CD31 expression)

As mentioned previously, after comparing cell behaviour within the three different hydrogels, endothelial cell culture was performed in microfluidic platforms, both in Matrigel® and Col/Fib gel. Similar to the previous cultures, several timepoints were set and cell morphology and CD31 expression were evaluated through immunocytochemistry. CD31, along with vascular endothelial cadherin (CD144), VEGF receptors, and von Willebrand factor (vWF), is a well-established marker for endothelial cell identification[85]. CD31 supports intercellular junctions and regulates paracellular permeability and angiogenesis. This molecule, besides being highly expressed in ECs, is also present in cells of the hematopoietic lineage[85]. Both Matrigel® and Col/Fib cultures were terminated at 24, 48 and 72 hours to assess the parameters discussed above.

Cells seeded within Matrigel® quickly formed similar structures to the ones observed during the 3D cultures in µ-Slide Angiogenesis, clearly visible at 24 hours, remaining stable throughout the 72 hours culture (Figure 26, white arrows). However, the intended 3D structure may be compromised due to detachment of the Matrigel® of the walls of the micro channels. This may occur due to Matrigel's degradation due to the high cell number and metabolic activity[91]. CD31 expression was noticeable across all three timepoints.

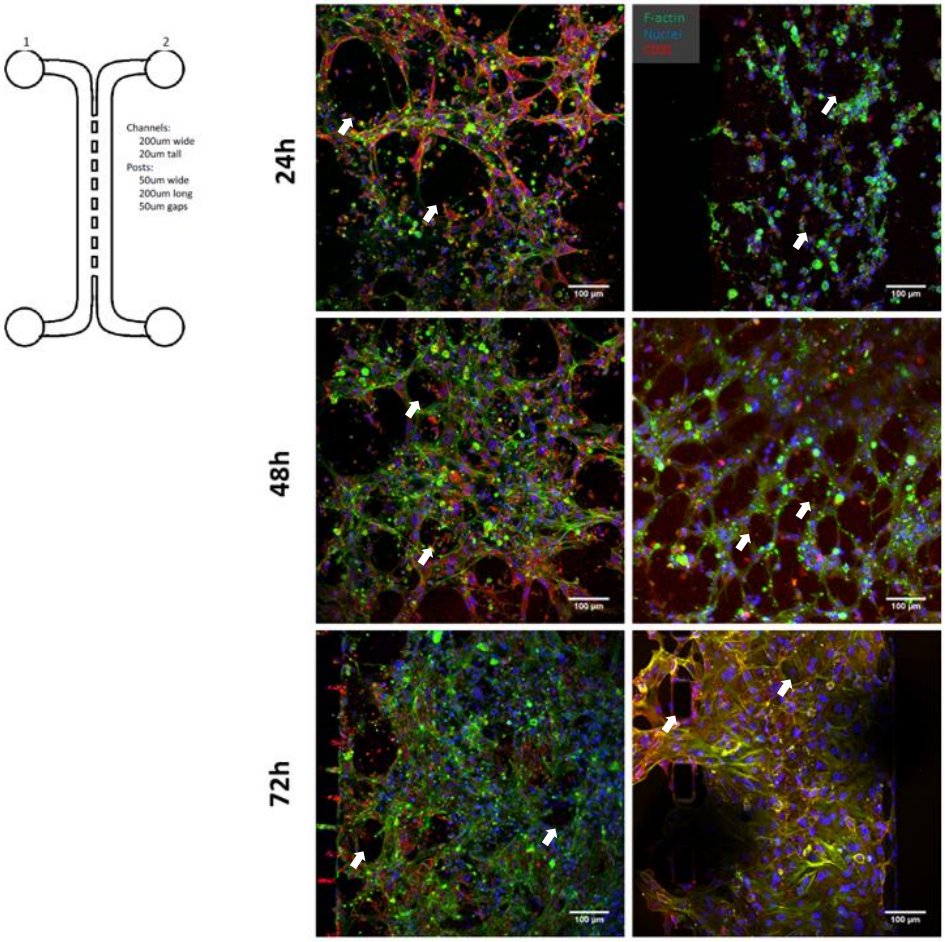

Figure 26-On the left: Design of the microfluidic platforms used for optimizing HUVECs culture within Matrigel® and Collagen/Fibrin hydrogels. Panel on the right: HUVECs culture in Matrigel® (left) and Col/Fib (right) hydrogels at different timepoints. Staining: green, F-actin; blue, nuclei; red, CD31.

Regarding the cells seeded in the Col/Fib gel, it was observed that rather than being within the gel in a 3D conformation, as intended, the cells coated the entirety of the microchannel walls (Figure 27).

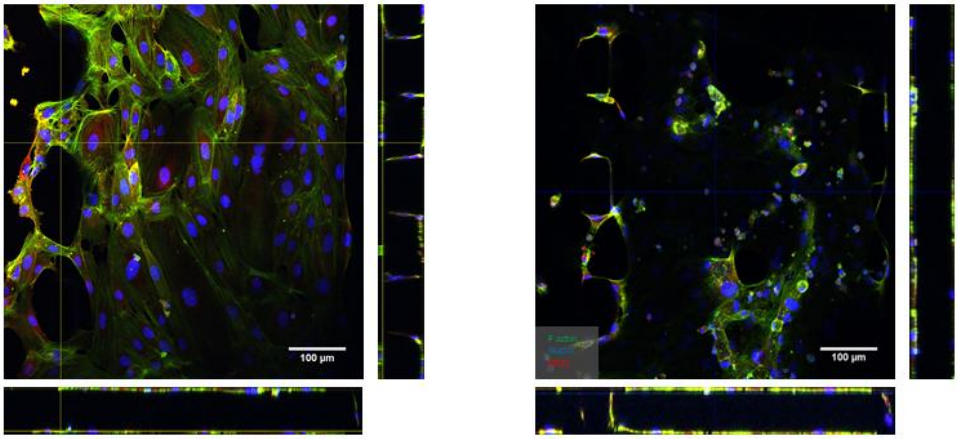

Figure 27 Microfluidic channels containing HUVECs cultured in Collagen/Fibrin hydrogel at 72 hours of culture. Orthogonal sections display HUVECs coating the microfluidic channel, as well as adhering to the micro grooves. Staining: green, F-actin; blue, nuclei; red, CD31.

Several studies have achieved the same organization within microfluidic platforms, but other strategies have been employed[69,94–96]. There has been a growing interest in developing strategies that allow the systematic formation of such ECs monolayers in microfluidic platforms, given its potential use in perfusion models, permeability assays and sprouting angiogenesis, transendothelial migration, cancer metastasis and innovative culture models[95]. Chung *et al.*[94], to mimic physiologically relevant 3D capillary morphogenesis, applied a surface treatment to PDMS microfluidic devices based on the precoating of a closed microfluidic channel with type I collagen. It was then observed that ECs had formed a monolayer within the scaffold compartment[94]. Zheng *et al.*[69]assembled microvascular networks within a native collagen type I matrix through by using a microstructured silicone stamp as a mold. The hydrogel was injected inside the mold and two collagen layers were sealed together to establish an enclosed structure. Cells were then seeded inside the collagen-coated device and the microvascular was formed after cell attachment[69]. Han *et al.*[95], from the same group that published the two previous mentioned reports, applied similar methodologies to reach the same level of microvascular organization. In other study[97], the microfluidic channels were consecutively coated with PDL, collagen type I and growth factor reduced Matrigel®. It was observed that cells formed a monolayer without detachment or sprouting, for more than 5 days of culture[97]. The same authors developed another strategy to assemble artificial microvascular architectures, based on hydrophobic patterning of hydrogels within a microfluidic channel[96]. The methodology employed to confine the hydrogel solution during the gelation process was the previous application of a butyl methacrylate-ethylene dimethacrylate (BMA-EDMA) pattering. This strategy allowed for the formation of a 3D extracellular matrix within the microchannel[96]. The authors further exemplified the employment of this technique in different contexts, namely 3D breast epithelial cancer cell migration studies, formation of a quiescent 3D blood capillary model and study of differentiation of human neural stem cells and MSCs[96]. Wipff *et al.*[98] published a report in which different functionalization methods are employed to bind extracellular matrix proteins, namely collagen, to PDMS. The study focused on the validation of a surface treatment that allows covalent binding of collagen to PDMS through oxygen plasma treatment, binding of 3-aminopropyltriethoxysilane to the oxidized surface and then covalent cross-linking of collagen using glutaraldehyde. This method is then compared to electrostatic LDL-functionalized PDMS and PDMS functionalized through collagen adsorption[98]. During that study, the condition in which collagen adsorbed to PDMS was

able to promote cell attachment, development of adhesion structures and cell proliferation, although to a lesser extent when compared to the remaining conditions. Nevertheless, the coating observed within the microchannels may have been caused by the same adsorption mechanism displayed in this study[98].

In our particular experiment, prior to the seeding of ECs, within the Col/Fib hydrogel, no surface treatment was applied to the microfluidic platform, therefore the microchannels coating observed was not expected. However, due to rapid polymerization, the hydrogel might have adhered to the walls of the microchannels, thereby promoting faster cell adhesion surrounding the channels.

It was also noticeable a significant contraction and detachment of the gel (Figure 28). The contraction of collagen I by ECs is described in the literature[99]. Liu *et al.*[99] have described that this event occurs as a consequence of the ability of ECs to remodel the surrounding ECM and is modulated by hemin, a CO donor. This effect is more pronounced when the number of cells increases, but is decreased when the collagen content within the gel formulation is increased[99]. The detachment of the hydrogel was not uniform across the microchannels, since there were areas where contraction was not observed. Nonetheless, through two similar 3D setups, two different cell organization types were successfully obtained inside the microfluidics.

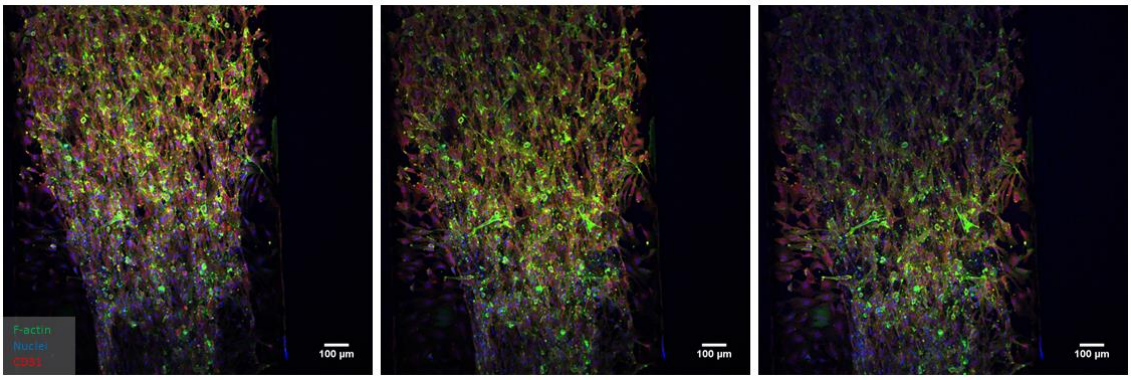

Figure 28-Different Z-stacks sections of HUVECs culture in Collagen/Fibrin hydrogel inside a microfluidic platform, showing hydrogel contraction. T=72h. Staining: green, F-actin; blue, nuclei; red, CD31.

Coculture of sensory neurons and endothelial cells

After successfully establishing an endothelial cell culture within both Matrigel® and Col/Fib hydrogels in the microfluidic platforms, a DRG-ECs co-culture was assembled. The strategy of platform design , pioneered by Park *et al.*[64], but already employed in more recent studies[58,65,100] allows for axonal outgrowth from the somal side to the axonal side. The microfluidic devices used in this dissertation (Figure 29) were designed to assemble a triculture model while mimicking the anatomical organization of the bone microenvironment. The somal side, separated from the other two compartments by microgrooves, is destined for the culture of DRG. This microgroove "bridge" allows for the outgrowth of nerve fibers from the somal to the axonal side, but not cell bodies, therefore establishing the communication between the DRG and other cell types to be seeded within the remaining compartments. Given the close interaction between blood nerve fibers and blood vessels, the middle compartment is meant for the culture of ECs in a 3D substrate. This compartment is separated from the osteogenic compartment by micro posts meant to prevent overflow of the substrate from a compartment to the other, thereby limiting each cell type to one compartment, while still allowing for cell contact and paracrine signalling. Prior the assembling of the DRG-ECs-osteoclasts triculture, a DRG-ECs co-culture was established. The DRG was seeded in the somal side, while the ECs were seeded in the axonal compartment. ECs were seeded within a 3D Matrigel® matrix, similar to the previous experiments.

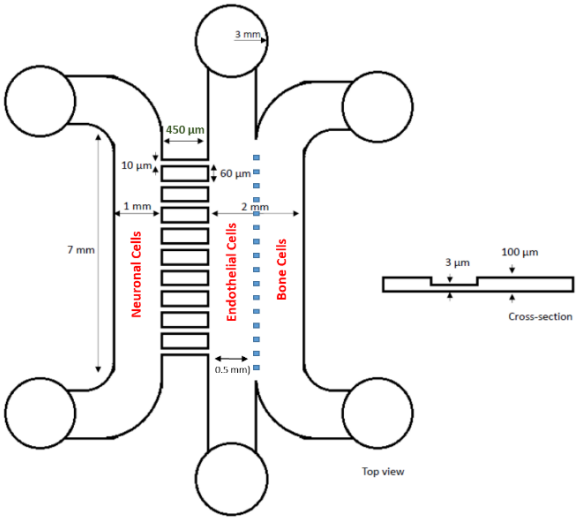

Figure 29- Microfluidic design projected for bone organotypic 3D triculture. Platforms employing this design were used to perform a Dorsal Root Ganglion-Endothelial cells co-culture.

In the DRG-Endothelial cell co-culture herein present, after 48 hours of culture, axonal outgrowth from the DRG compartment to the endothelial cell compartment was observable through immunofluorescence of ßIII tubulin, a neuronal specific marker (Figure 30). Nakahashi *et al.*[101] have reported the presence of brain-derived neurotrophic factor (BDNF) both in HUVECs culture and their culture medium. BDNF is a neurothrophin found in the brain and peripheral nerves linked to neural development, survival and repair upon injury occurrence[101]. Furthermore, the authors described that while the expression of BDNF is upregulated by the and rising of intracellular cAMP levels, its down-regulation carried out by Ca^{2+} ionophore, bovine brain extract and laminar fluid shear stress. More recently, Yuan *et al.*[102] have shown a that DRG display greater biological activity when co-culture with human microvascular endothelial cells (HMVEC) and further investigated the mechanism responsible by this effect, in a follow up study[103]. Through the assembling of a co-culture Transwell model between DRG and HMVEC, the authors reported that the upregulation of regeneration and differentiation markers on DRGs is partially due to the secretion of BDNF by HMVECs[103]. The effects reported by these studies and their underlying mechanisms may explain the axonal outgrowth here observed. However, further optimization of the co-culture is required for more in-depth studies. Despite its potent angiogenic effect, Matrigel® present disadvantages, when compared to other substrates such as fibrin or collagen, namely the inability to control the exact amount of growth factors present within the formulation and batch variability[104]. The establishment of a DRG-ECs co-culture, in which ECs are cultured within the Col/Fib gel above mentioned would mitigate these specific disadvantages of Matrigel®. Once

co-culture optimization is conducted, axonal outgrowth quantification as well as functional studies of the neurites through assessment of CGRP presence can be performed[65].

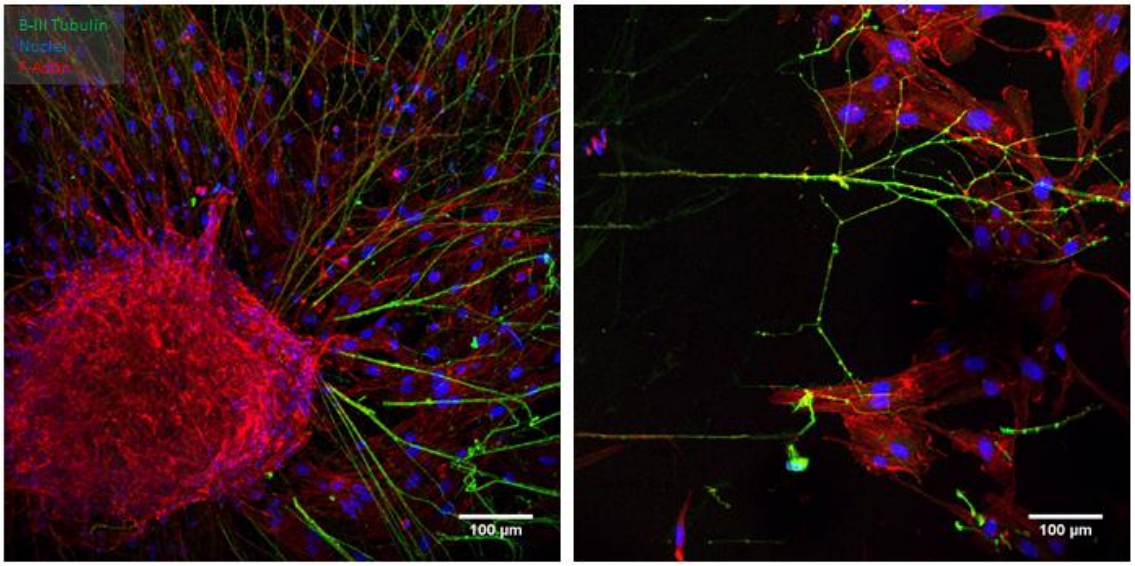

Figure 30- Dorsal Root Ganglion-Endothelial cells co-culture. DRG on the left. Neurite projection from the somal to the axonal compartment (right). Staining: green, ß-III tubulin; blue, nuclei; red, F-actin.

Triculture of sensory neurons, endothelial cells and osteoclasts

The next step, and main goal of this dissertation, was the assembling of a triculture model comprised of sensory neurons, ECs and osteoclasts within a microfluidic device, thereby mimicking the bone microenvironment and recapitulating cell interactions that occur *in vivo*.

Like the previous assembled DRG-ECs co-culture, the DRG was seeded on the somal side. On the axonal side, ECs were seeded either in Col/Fib (Figure 31) or Matrigel® (Figure 32) substrates, in a 3D manner, at a 20 x 10^6 cells/ml density. On the bone cell compartment, 5 x10^4 osteoclasts were seeded, in a 2D conformation.

Several technical difficulties have been encountered, particularly during cell seeding. The first and major difficulty was found during the loading of the substrates to the micro channels. In both Matrigel® and Col/Fib conditions, the hydrogel flooded the bone cell compartment. This might have occurred due to the sealing performed through oxygen plasma treatment, which has been reported to alter surface properties of the PDMS[105]. During this method, polar functional groups were generated, thereby converting the hydrophobic surface into an hydrophilic one[105].To overcome this problem, an attempt to aspirate the excess of hydrogel from the bone cell compartment was made. Different results were obtained depending on the hydrogel used. In the case of Matrigel®, it was possible to aspirate the excess of substrate within the bone compartment. On the other hand, in the case of the Col/Fib substrate, since the hydrogel polymerized faster, this was not successful, and the gel was confined to both the ECs compartment and the bone cells compartment. In neither case the resulting conditions were ideal. In the case of Matrigel®, even though the removal of excess hydrogel was accomplished, cell content may also have been removed from the ECs compartment, thus altering the number of cells present within the microfluidic device. In the case of the Col/Fib hydrogel, ECs were confined to both the ECs compartment and the bone cells compartment and no spatial separation of osteoclasts and ECs was achieved, contrary to the initial planning. The issue herein reported may be mitigated by slightly changing the design of the microfluidic platform. To expand the length of the posts between the ECs compartment and bone cells compartment may help preventing the hydrogels from invading the adjacent compartment. Despite

these difficulties, the culture in both Matrigel® and Col/Fib hydrogels was extended for 96 hours. In the somal compartment, explants from embryonic DRG were cultured.

At the 96 hours timepoint, cell morphology and organization, HUVECs CD31 expression and axonal outgrowth were analyzed. Despite the reported positive effects of ECs on the development of DRG[103], and the promotion of axonal outgrowth by osteoclasts[58], after 96 hours of culture there was no axonal outgrowth was observed from the somal compartment to the axonal compartment, independently of the substrate used for the HUVEC culture. In the microfluidic devices where HUVECs were seeded within the Col/Fib hydrogel, it was noticeable the distribution of the substrate, and consequently HUVECs, across both compartments. The presence of HUVECs was distinguishable through the expression of CD31. Similar to previous results, HUVECs were found to be coating the micro channels walls, and hydrogel retraction was also observable (Figure 31). Together with the previous results from the monoculture, it was shown that Col/Fib hydrogels adhered to PDMS both with and without PDL coating. The osteoclasts, seeded after the hydrogel polymerization, appeared distributed across both compartments as well. Their morphology, observed through F-actin staining, was significantly different from expanding osteoclasts cultured in α-MEM with 10% FBS (Figure 33), characterized by the existence of large multinucleated cells. In the triculture, osteoclasts displayed a small, round morphology, possibly indicating cell death[106]. Regarding the condition in which HUVECs were seeded within Matrigel®, the same observations can be made regarding CD31 expression and axonal outgrowth (Figure 32). As for the osteoclast compartment, the existence of ECs was not as pronounced as in the Col/Fib condition, but the observations made respecting the osteoclasts morphology and possible cell death remain.

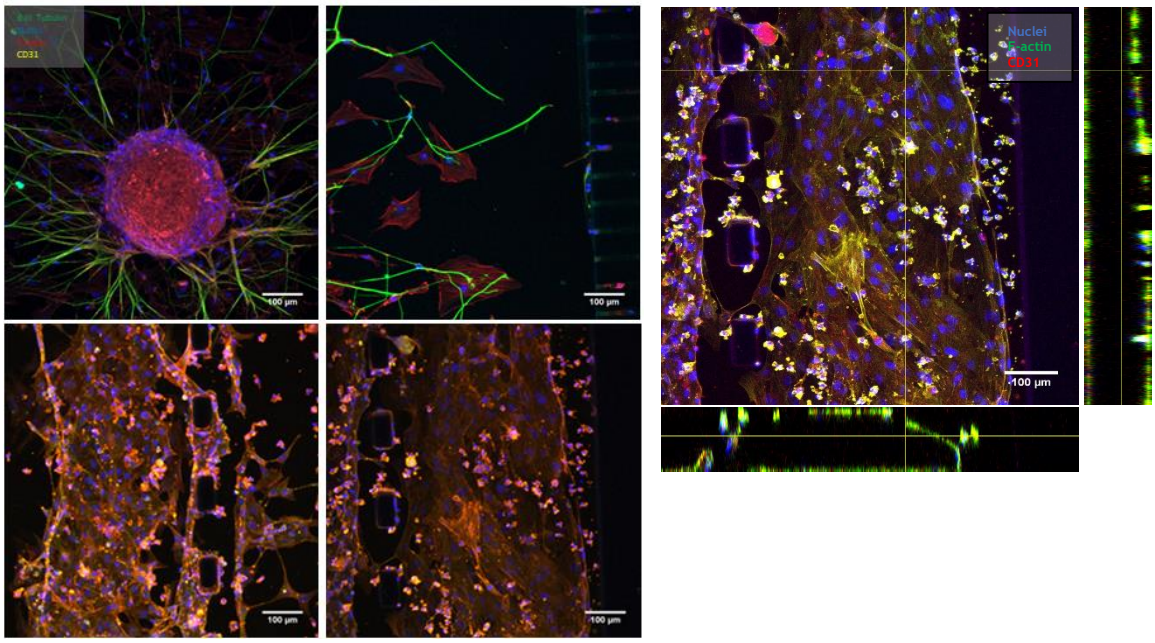

Figure 31- Left panel- staining for ß-tubulin (green), nuclei (blue), F-actin (red) and CD31 (yellow). The top images represent the somal side: Dorsal Root Ganglion (left) and axonal outgrowth (right). Bottom images represent the axonal side with HUVECs seeded within Collagen/Fibrin hydrogel occupying both compartments. Right figure-orthogonal section of axonal compartment: osteoclasts and HUVEC are present. It is possible to observe HUVEC coating the micro channel, as well as hydrogel retraction.

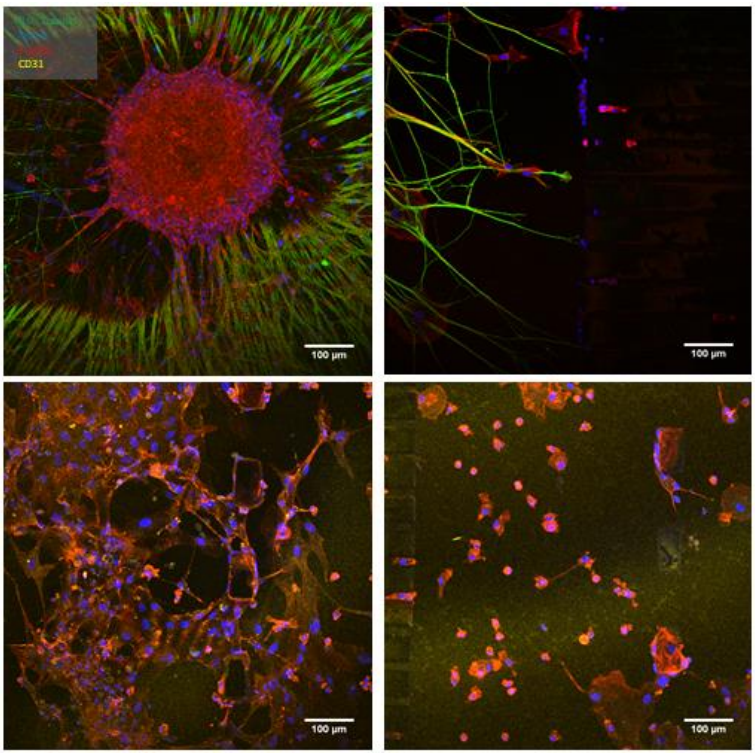

Figure 32- Staining for ß-tubulin (green), nuclei (blue), F-actin (red) and CD31 (yellow). The top images represent the somal side: Dorsal Root Ganglion (left) and axonal outgrowth (right). Bottom images represent the axonal side with HUVECs seeded within Matrigel®.

Angiogenic potential of osteoclasts

Angiogenesis has a key role during bone development, homeostasis and repair. Bone has been shown to be a highly vascularized organ with a specific capillary network. The osteoclasts are found in close proximity with capillaries during bone development and fracture healing. The existent spatial and temporal proximity between these two players in bone homeostasis suggests underlying interactions between these two cell types. Moreover, some reports describe endothelial progenitor cells to promote survivability, migration and differentiation of osteoclast precursors[37], while others have shown that endothelial cell produced netrin-4 inhibited osteoclast differentiation[39]. A recent transwell co-culture study[107] further reported impaired osteoclast differentiation in HUVECs-Osteclasts co-cultures[107].

Osteoclast contribution towards angiogenesis and its underlying mechanisms remain to be fully elucidated. With the purpose of studying a potential paracrine effect of osteoclasts in ECs, a 2D tube formation assay was performed. This assay is widely used as a first screen for pro or anti-angiogenic factors because it is easy to perform, rapid and allows for high throughput analysis[82]. HUVECs were seeded on top of Corning® BioCoat™ Matrigel® Matrix Thin-Layer 96 well plate (cell density of 6400 cells/cm^2) and treated with human osteoclast (hOC) conditioned medium (CM). CM was collected from osteoclasts previously plated in different conditions: hOC plated-on tissue culture polystyrene (TCPS) with α-MEM supplemented with either 10% -hOC CM(10)- or 0,5%-hOC CM (0,5)-FBS (Figure 33), and hOC plated-on top of bone slices-hOC (BS)-, simulating *in vivo* bone resorption. Since FBS possesses a large number of nutritional and macromolecular growth factors[108], the purpose of using a lower FBS concentration was to avoid masking any effect of possible molecules secreted by osteoclasts. The remaining conditions were composed of α-MEM with 10%- α-MEM (10)- or 0,5%-α-MEM (0,5)- FBS since the hOC CM was obtained with different formulations of α-MEM. The inclusion of the α-MEM of similar formulation, but with no contact with hOC, was meant to assess if this medium would have any effect on HUVECs. In the positive control, cells were plated with EGM™-2 Endothelial Cell Growth Medium. Pictures of each well were acquired at 0, 3, 6, 9 and 24 hours timepoints.

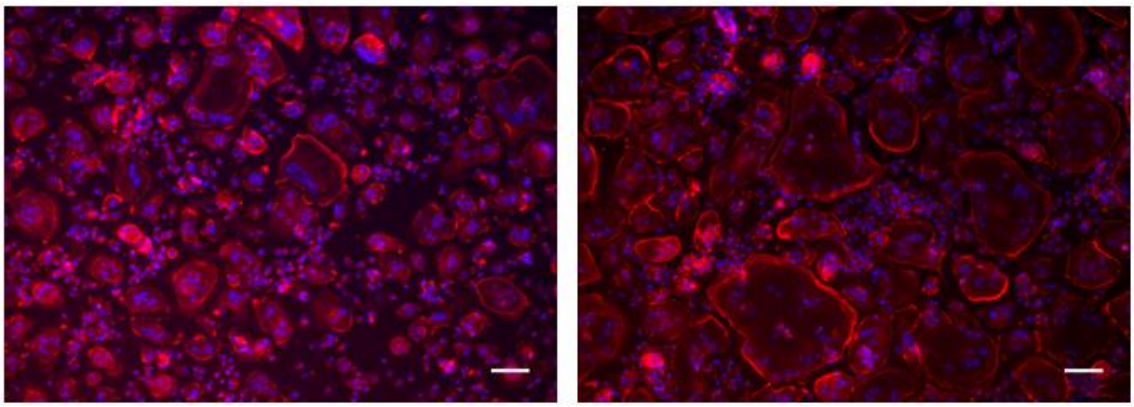

Figure 33- hOC: staning for F-actin (red) and nuclei (blue): α-MEM 0,5% FBS (left); α-MEM 10% FBS (right), large and more numerous osteoclasts are present. Scale: 100µm.

The readouts of the 2D tube formation assay, as mentioned previously, on the first section of the Results and Discussion, are based on the quantification of different parameters such as number of tubes; number of loops; number of branch nodes and length of tubes[86]. In the present experiment no tube formation occurred. A possible explanation for this might be cell density chosen. Several authors claim cell density to be a critical parameter regarding tube formation. The cell density herein used has been shown to result in the formation of tubular like structures[82,109,110], and was a result of adaptation of manufacturer's tube formation protocol (Ibidi). However others advise the use of lower cell densities ($4{,}8x10^4$ cells/cm^2) [82,84,86,111].

Even though no quantification was performed on these data, by observation of each time point for each condition, qualitative information was drawn from this experiment (Figure 34). It was possible to observe that, while there was no tube formation even within the EGM-2 cultured HUVECs, cells retained their regular morphology throughout the 24-hour culture period, presenting a spread shape already at the 3 hours timepoint that was kept until the 24 hours. HUVECs seeded with α-MEM (10) showed similar results to the positive control (although at 24 hours the positive control presented more elongated cells), possibly indicating that the osteoclast basal culture medium is not harmful to HUVECs. In contrast with the positive, HUVECs cultured with α-MEM (0,5) presented a round shape at the 3-hour timepoint, possibly due to lack of cell adhesion to the well and consequent apoptotic state. Given the previous observations about the α-MEM (10) condition, the cell death observed in the α-MEM (0,5) condition might be due to the low FBS concentration. Contrary to its respective control, within the hOC CM (0,5) condition, the presence of living cells indicates that soluble factors secreted by osteoclasts may support the culture of HUVECs. In fact, a report has attributed osteopontin a positive effect on endothelial cell activity[41]. The culture of HUVECs with hOC CM (10), the cells seemed to be stretched, similar to the positive control. This condition also showed some cell aggregate, possibly due to the high number of cells due to poor distribution of cells

across the well. Regarding the hOC CM (BS) condition, where the release of matrix factors was expected, no improvement was observed when compared with remaining hOC CM conditions. Across all hOC CM conditions, there seemed to be cell mobilization, although no structures were formed. Staining for CD31, F-actin and nuclei would improve visualization of cell structures.

To understand if the interaction between myeloma cells and osteoclasts enhanced angiogenesis, Tanaka *et al.*[41] performed tube formation assays with HUVECs seeded on top of collagen type I treated with hOC CM (α-MEM supplemented with 10% FBS) and CM from hOC and myeloma cells co-culture. The authors reported the CM from hOC cultures to enhance angiogenesis *in vitro* and that this stimulation was increased in the case of CM from the co-cultures[40,41]. Through antibody neutralization, the authors identified the osteoclast-derived angiogenesis to be attributed to osteopontin and the myeloma cell-derived angiogenesis to be due to VEGF. However, Cackowski & Roodman[44] have questioned these results based on the unknown purity of hOC in cultures used in the experiments; the augmented angiogenic activity originated from the co-culture might be due to the additive effect of the combination of angiogenic factors produced by both cell types, and not due to cell interaction; the neutralizing antibody approach used raises ambiguity regarding the importance of different angiogenic factors, instead of identifying the most important of them[40]. Nevertheless, the results presented in the study of Tanaka *et al.*[41] have hint the existence of a paracrine effect of osteoclasts on ECs. Despite the unsuccessful attempt at performing the 2D tube assay, hOC CM (10) may have sustained the culture of HUVECs for 24 hours.

Besides the cell density adaptation, another optimization step may be applied. This would consist of concentrating hOC CM, to later dilute it in EGM-2. Since EGM-2 is appropriate for endothelial cell culture, by diluting concentrated hOC CM in EGM-2, it would be possible to study possible paracrine effects while increasing cell survivability. These optimization steps of this assay may help set a starting point to potentially better understand the role of osteoclasts in angiogenesis.

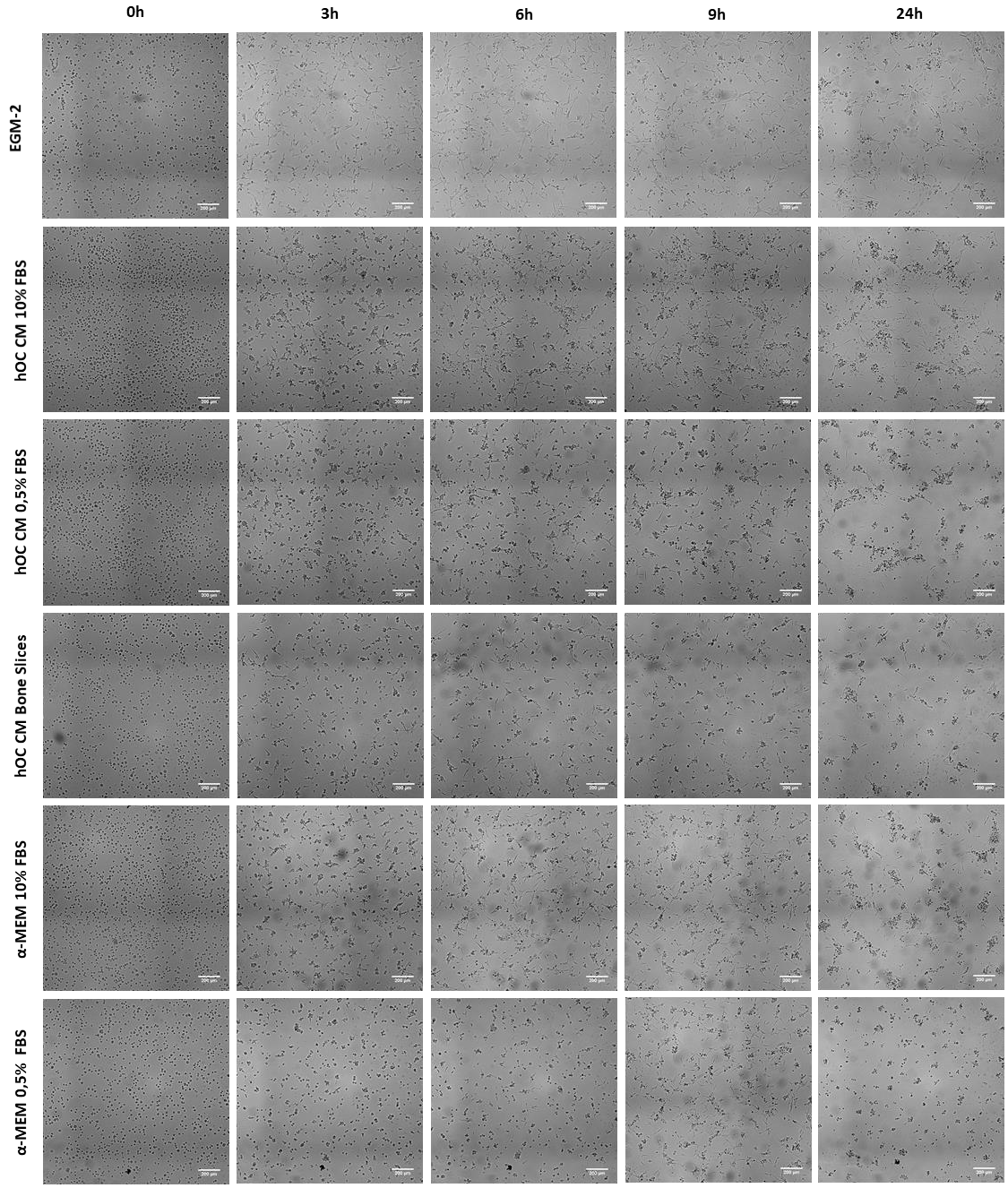

Figure 34- 2D Tube formation on top of Corning® BioCoat™ Matrigel® Matrix Thin-Layer 96. HUVECS were treated with hOC CM collected from previously plated hOC (50000 cells/well) for 3 days on top of: TCPS with α-MEM 0,5% FBS culture medium; TCPS with α-MEM 10% FBS culture medium; bone slices with α-MEM 10% FBS culture medium. The remaining conditions consisted of HUVECs treated with α-MEM 0,5% FBS culture medium, and α-MEM 10% FBS culture medium.

This page was intentionally left in blank

Chapter IV: Conclusion and Future Considerations

Throughout the present work, a step-by-step process was followed to establish an *in vitro* triculture model of sensory neurons, HUVECs, and human osteoclasts within a microfluidic platform. In addition, a tube formation assay was performed to study the paracrine effect of osteoclasts on ECs.

During the optimization of HUVEC culture, different hydrogels (Matrigel®, fibrin and Col/Fib) were compared. Matrigel® has been extensively used as a substrate to support the formation of vascular networks. Fibrin hydrogel was also tested given its natural angiogenic properties. Lastly, Col/Fib hydrogels have also been used since collagen type I is the main component of the organic fraction of bone matrix, making this hydrogel a prime candidate for a substrate to include in a vascularized bone model.

Optimal cell density was evaluated for the formation of vascular structures across the three substrates. Cells remained viable and metabolically active for an established culture period of 96 hours. Together with the previous reasoning, these observations led to the choice of Matrigel® and Col/Fib hydrogels as substrates to include in a bone mimicking vascularized model.

Respecting the optimized parameters, cells were successfully cultured within the microfluidic platforms. Different cell arrangement was observed in the two hydrogels. While in Matrigel®, cells presented the same morphology as observed in the 3D assays, in Col/Fib hydrogel conditions, cells coated the microchannels, forming a lumen-like structure.

The co-culture between sensory neurons and HUVECs was then performed. After 48 hours of culture, neurite projection from the somal compartment to the axonal side was observed, possibly indicating a positive effect of ECs on axonal outgrowth.

Following the previous co-culture, the assembling of a triculture between sensory neurons, ECs, and human osteoclasts. Due to experimental difficulties, the spatial separation between HUVECs and osteoclasts, and possibly viability, was compromised. Moreover, although sensory neurons grew out healthy, no axonal outgrowth was observed from the somal side to the axonal compartments. This might be explained by the difficulties previously stated. The triculture assembly requires further optimization, namely a possible redesign of the microfluidic device that would block gel extravasion from one compartment to the other, while still allowing cell communication.

Besides the optimization steps referred previously, other aspects of triculture assemble can be improved. ECs are often co-cultured with mural cells to improve the maturation and stabilization of vascular networks. In the present case, no mural cells are present, but murals cells-secreted factors, such as angiopoietins, may be added to the culture medium to recreate the same effect. In addition, culture of ECs under flow would be a more realistic representation of vasculature, since it is described in the literature that flow influences EC differentiation. Also, the hydrogel formulation could be altered to include a mineralized component, mimicking the bone microenvironment with greater detail. It would be of the utmost interest to culture the human osteoclasts within a 3D manner, within the optimized Col/Fib hydrogel, stimulating the osteoclast bone resorbing activity found *in vivo*. Once fully optimized, other specific cell activities may be analyzed, such as neurite projection, evaluation of vascular networks and resorbing activity of osteoclasts. These analyses may help understand how these cells interact and influence each other.

To unravel the possible paracrine effect of osteoclasts on ECs, a 2D tube formation assay was performed, in which HUVEC were treated with human osteoclast conditioned medium. No tube formation was observed, possibly due to inappropriate cell density. However, it was possible to observe that osteoclast conditioned medium might promote HUVEC survivability through paracrine signaling. In the future, cell density must be optimized to achieve tube formation. In addition, other optimization step may include concentrate the osteoclast conditioned medium to further dilute it in HUVEC basal medium, thereby allowing for evaluation of possible paracrine effects, without impairing cell viability.

The proper assembling of a triculture model could be a powerful tool to study and possibly unravel the mechanisms implied in the interactions between innervation, vascularization, and osteoclastogenesis. Since these three processes have been associated with pathological conditions leading to pain and enhance bone destruction, unveiling these interactions might ultimately lead to the development of therapies to eliminate these effects.

References

1. Grabowski, P. Physiology of bone. *Calcium Bone Disord. Child. Adolesc. Second Ed.* **28,** 33–55 (2015).
2. Florencio-Silva, R., Sasso, G. R. da S., Sasso-Cerri, E., Simões, M. J. & Cerri, P. S. Biology of Bone Tissue: Structure, Function, and Factors That Influence Bone Cells. *Biomed Res. Int.* **2015,** 421746 (2015).
3. Salgado, A. J., Coutinho, O. P. & Reis, R. L. Bone tissue engineering: State of the art and future trends. *Macromol. Biosci.* **4,** 743–765 (2004).
4. Scheinpflug, J. *et al.* Journey into Bone Models: A Review. *Genes (Basel).* **9,** 247 (2018).
5. Bellido, T. Osteocyte-driven bone remodeling. *Calcif. Tissue Int.* **94,** 25–34 (2014).
6. Rutkovskiy, A., Stensløkken, K.-O. & Vaage, I. J. Osteoblast Differentiation at a Glance. *Med. Sci. Monit. Basic Res.* **22,** 95–106 (2016).
7. Sims, N. A. & Gooi, J. H. Bone remodeling: Multiple cellular interactions required for coupling of bone formation and resorption. *Semin. Cell Dev. Biol.* **19,** 444–451 (2008).
8. Hayashi, M., Nakashima, T., Taniguchi, M., Kodama, T. & Kumanogoh, A. Osteoprotection by semaphorin 3A. *Nature* **485,** 69–74 (2012).
9. Hadjidakis, D. J. & Androulakis, I. I. Bone remodeling. *Ann. N. Y. Acad. Sci.* **1092,** 385–396 (2006).
10. Charles, J. F. & Aliprantis, A. O. Osteoclasts: More than 'bone eaters'. *Trends Mol. Med.* **20,** 449–459 (2014).
11. Cappariello, A., Maurizi, A., Veeriah, V. & Teti, A. Reprint of: The Great Beauty of the osteoclast. *Arch. Biochem. Biophys.* **561,** 13–21 (2014).
12. Silver, I. A., Murrills, R. J. & Etherington, D. J. Microelectrode studies on the acid microenvironment beneath adherent macrophages and osteoclasts. *Exp. Cell Res.* **175,** 266–276 (1988).
13. Lindsey, A. E. *et al.* Functional expression and subcellular localization of an anion exchanger cloned from choroid plexus. *Proc. Natl. Acad. Sci. U. S. A.* **87,** 5278–82 (1990).
14. Teti, A. *et al.* Cytoplasmic pH regulation and chloride/bicarbonate exchange in avian osteoclasts. *J. Clin. Invest.* **83,** 227–33 (1989).
15. Van Wesenbeeck, L. *et al.* Involvement of PLEKHM1 in osteoclastic vesicular transport and osteopetrosis in incisors absent rats and humans. *J. Clin. Invest.* **117,** 919–30 (2007).
16. Teti, A. Mechanisms of osteoclast-dependent bone formation. *Bonekey Rep.* **2,** 1–6 (2013).
17. Hayman, A. R. & Cox, T. M. Tartrate-Resistant Acid Phosphatase Knockout Mice. *J. Bone Miner. Res.* **18,** 1905–1907 (2003).
18. Zhao, C. *et al.* Bidirectional ephrinB2-EphB4 signaling controls bone homeostasis. *Cell Metab.* **4,** 111–121 (2006).
19. Chen, X. *et al.* Osteoblast–osteoclast interactions. *Connect. Tissue Res.* **59,** 99–107 (2018).
20. Lee, S.-H. *et al.* v-ATPase V0 subunit d2–deficient mice exhibit impaired osteoclast fusion and increased bone formation. *Nat. Med.* **12,** 1403–1409 (2006).
21. Kusu, N. *et al.* Sclerostin Is a Novel Secreted Osteoclast-derived Bone Morphogenetic Protein Antagonist with Unique Ligand Specificity. *J. Biol. Chem.* **278,** 24113–24117 (2003).
22. Ota, K. *et al.* Sclerostin is expressed in osteoclasts from aged mice and reduces osteoclast-mediated stimulation of mineralization. *J. Cell. Biochem.* **114,** 1901–1907 (2013).
23. Martin, T. J. Coupling factors: How many candidates can there be? *J. Bone Miner. Res.* **29,** 1519–1521 (2014).
24. Takeshita, S. *et al.* Osteoclast-secreted CTHRC1 in the coupling of bone resorption to formation. *J. Clin. Invest.* **123,** 3914–3924 (2013).
25. Vu, T. H. *et al.* MMP-9/gelatinase B is a key regulator of growth plate angiogenesis and

apoptosis of hypetrophic chondrocytes. *Cell* **93,** 411–422 (1998).
26. Hall, B. K. & Miyake, T. All for one and one for all: Condensations and the initiation of skeletal development. *BioEssays* **22,** 138–147 (2000).
27. Karaplis, A. C. Chapter 3 – Embryonic Development of Bone and Regulation of Intramembranous and Endochondral Bone Formation. in *Principles of Bone Biology* 53–84 (2008).
28. Franz-Odendaal, T. A. Induction and patterning of intramembranous bone. *Front. Biosci. (Landmark Ed.* **16,** 2734–46 (2011).
29. Sivaraj, K. K. & Adams, R. H. Blood vessel formation and function in bone. *Development* **143,** 2706–15 (2016).
30. Kanczler, J. M. & Oreffo, R. O. C. Osteogenesis and angiogenesis: The potential for engineering bone. *Eur. Cells Mater.* **15,** 100–114 (2008).
31. Maes, C. Role and regulation of vascularization processes in endochondral bones. *Calcif. Tissue Int.* **92,** 307–323 (2013).
32. Grosso, A. *et al.* It Takes Two to Tango: Coupling of Angiogenesis and Osteogenesis for Bone Regeneration. *Front. Bioeng. Biotechnol.* **5,** 1–7 (2017).
33. Ramasamy, S. K. Structure and Functions of Blood Vessels and Vascular Niches in Bone. *Stem Cells Int.* **2017,** (2017).
34. Niida, S. *et al.* Vascular endothelial growth factor can substitute for macrophage colony-stimulating factor in the support of osteoclastic bone resorption. *J. Exp. Med.* **190,** 293–8 (1999).
35. Helmrich, U. *et al.* Osteogenic graft vascularization and bone resorption by VEGF-expressing human mesenchymal progenitors. *Biomaterials* **34,** 5025–5035 (2013).
36. Collin-Osdoby, P. *et al.* Receptor activator of NF-kappa B and osteoprotegerin expression by human microvascular endothelial cells, regulation by inflammatory cytokines, and role in human osteoclastogenesis. *J. Biol. Chem.* **276,** 20659–72 (2001).
37. Pang, H. *et al.* Co-culture with endothelial progenitor cells promotes survival, migration, and differentiation of osteoclast precursors. *Biochem. Biophys. Res. Commun.* **430,** 729–734 (2013).
38. CHIKATSU, N. *et al.* Clonal Endothelial Cells Produce Humoral Factors that Inhibit Osteoclast-Like Cell Formation In Vitro. *Endocr. J.* **49,** 439–447 (2002).
39. Enoki, Y. *et al.* Netrin-4 derived from murine vascular endothelial cells inhibits osteoclast differentiation in vitro and prevents bone loss in vivo. *FEBS Lett.* **588,** 2262–2269 (2014).
40. CACKOWSKI, F. C. & ROODMAN, G. D. Perspective on the Osteoclast: An Angiogenic Cell? *Ann. N. Y. Acad. Sci.* **1117,** 12–25 (2007).
41. Tanaka, Y. *et al.* Myeloma cell-osteoclast interaction enhances angiogenesis together with bone resorption: A role for vascular endothelial cell growth factor and osteopontin. *Clin. Cancer Res.* **13,** 816–823 (2007).
42. Bergers, G. *et al.* Matrix metalloproteinase-9 triggers the angiogenic switch during carcinogenesis. *Nat. Cell Biol.* **2,** 737–744 (2000).
43. Engsig, M. T. *et al.* Matrix metalloproteinase 9 and vascular endothelial growth factor are essential for osteoclast recruitment into developing long bones. *J. Cell Biol.* **151,** 879–89 (2000).
44. Cackowski, F. C. *et al.* Osteoclasts are important for bone angiogenesis. *Blood* **115,** 140–149 (2010).
45. Cao, X. PDGF-BB secreted by preosteoclasts induces angiogenesis during coupling with osteogenesis. *Nat. Med.* **20,** 1270–1278 (2014).
46. Kusumbe, A. P. & Adams, R. H. Osteoclast progenitors promote bone vascularization and osteogenesis. *Nat. Med.* **20,** 1238–1240 (2014).
47. Franquinho, F. *et al.* Neuropeptide Y and osteoblast differentiation - the balance between the neuro-osteogenic network and local control. *FEBS J.* **277,** 3664–3674 (2010).
48. Gkiatas, I. *et al.* The Multifactorial Role of Peripheral Nervous System in Bone Growth. *Front. Phys.* **5,** 1–6 (2017).
49. Edoff, K., Hellman, J., Persliden, J. & Hildebrand, C. The developmental skeletal growth in the rat foot is reduced after denervation. *Anat. Embryol. (Berl).* **195,** 531–538 (1997).

50. Song, D. *et al*. Denervation impairs bone regeneration during distraction osteogenesis in rabbit tibia lengthening. *Acta Orthop.* **83,** 406–410 (2012).
51. Marrella, A. *et al*. Engineering vascularized and innervated bone biomaterials for improved skeletal tissue regeneration. *Mater. Today* **21,** 362–376 (2018).
52. Akopian, A. *et al*. Effects of CGRP on human osteoclast-like cell formation: A possible connection with the bone loss in neurological disorders? *Peptides* **21,** 559–564 (2000).
53. Russell, F. A., King, R., Smillie, S.-J., Kodji, X. & Brain, S. D. Calcitonin Gene-Related Peptide: Physiology and Pathophysiology. *Physiol. Rev.* **94,** 1099–1142 (2014).
54. Elefteriou, F. Regulation of bone remodeling by the central and peripheral nervous system. *Arch. Biochem. Biophys.* **473,** 231–236 (2008).
55. Schinke, T. *et al*. Decreased bone formation and osteopenia in mice lacking α-calcitonin gene-related peptide. *J. Bone Miner. Res.* **19,** 2049–2056 (2004).
56. Goto, T., Yamaza, T., Kido, M. A. & Tanaka, T. Light- and electron-microscopic study of the distribution of axons containing substance P and the localization of neurokinin-1 receptor in bone. *Cell Tissue Res.* **293,** 87–93 (1998).
57. Mori, T. *et al*. Substance P Regulates the Function of Rabbit Cultured Osteoclast; Increase of Intracellular Free Calcium Concentration and Enhancement of Bone Resorption. *Biochem. Biophys. Res. Commun.* **262,** 418–422 (1999).
58. Neto, E. *et al*. Osteoclasts control sensory neurons axonal growth through epidermal growth factor receptor signaling. *bioRxiv* (2018).
59. Mapp, P. I. & Walsh, D. A. Mechanisms and targets of angiogenesis and nerve growth in osteoarthritis. *Nat. Rev. Rheumatol.* **8,** 390–398 (2012).
60. Bone, E. *et al*. NGF-TrkA Signaling by Sensory Nerves Coordinates the Vascularization and Ossification of Developing Article NGF-TrkA Signaling by Sensory Nerves Coordinates the Vascularization and Ossification of Developing Endochondral Bone. *CellReports* **16,** 2723–2735 (2016).
61. Sackmann, E. K., Fulton, A. L. & Beebe, D. J. The present and future role of microfluidics in biomedical research. *Nature* **507,** 181–189 (2014).
62. Neto, E. *et al*. Compartmentalized Microfluidic Platforms: The Unrivaled Breakthrough of In Vitro Tools for Neurobiological Research. *J. Neurosci.* **36,** 11573–11584 (2016).
63. Bhatia, S. N. & Ingber, D. E. Microfluidic organs-on-chips. *Nat. Biotechnol.* **32,** 760–772 (2014).
64. Park, J. W., Vahidi, B., Taylor, A. M., Rhee, S. W. & Jeon, N. L. Microfluidic culture platform for neuroscience research. *Nat. Protoc.* **1,** 2128–2136 (2006).
65. Neto, E. *et al*. Sensory neurons and osteoblasts: close partners in a microfluidic platform. *Integr. Biol.* **6,** 586–595 (2014).
66. Stegen, S. & Carmeliet, G. The skeletal vascular system – Breathing life into bone tissue. *Bone* 1–9 (2017).
67. Blache, U. & Ehrbar, M. Inspired by Nature: Hydrogels as Versatile Tools for Vascular Engineering. *Adv. Wound Care* **7,** 232–246 (2018).
68. Wong, K. H. K., Chan, J. M., Kamm, R. D. & Tien, J. Microfluidic Models of Vascular Functions. *Annu. Rev. Biomed. Eng.* **14,** 205–230 (2012).
69. Zheng, Y. *et al*. In vitro microvessels for the study of angiogenesis and thrombosis. *Proc. Natl. Acad. Sci. U. S. A.* **109,** 9342–7 (2012).
70. Miller, J. S. *et al*. Rapid casting of patterned vascular networks for perfusable engineered three-dimensional tissues. *Nat. Mater.* **11,** 768–774 (2012).
71. Rouwkema, J. & Khademhosseini, A. Vascularization and Angiogenesis in Tissue Engineering: Beyond Creating Static Networks. *Trends Biotechnol.* **34,** 733–745 (2016).
72. Jeon, J. S. *et al*. Generation of 3D functional microvascular networks with human mesenchymal stem cells in microfluidic systems. *Integr. Biol.* **6,** 555–563 (2014).
73. Bersini, S. *et al*. A microfluidic 3D invitro model for specificity of breast cancer metastasis to bone. *Biomaterials* **35,** 2454–2461 (2014).
74. Jusoh, N., Oh, S., Kim, S., Kim, J. & Jeon, N. L. Microfluidic vascularized bone tissue model with hydroxyapatite-incorporated extracellular matrix. *Lab Chip* **15,** 3984–3988 (2015).
75. Torisawa, Y. *et al*. Bone marrow–on–a–chip replicates hematopoietic niche physiology in vitro. *Nat. Methods* **11,** 663–669 (2014).
76. Sun, Q. *et al*. Ex vivo replication of phenotypic functions of osteocytes through

biomimetic 3D bone tissue construction. *Bone* **106,** 148–155 (2018).
77. Morin, K. T. & Tranquillo, R. T. In vitro models of angiogenesis and vasculogenesis in fi brin gel. *Exp. Cell Res.* **319,** 2409–2417 (2013).
78. Bongio, M., Lopa, S., Gilardi, M., Bersini, S. & Moretti, M. A 3D vascularized bone remodeling model combining osteoblasts and osteoclasts in a CaP nanoparticle-enriched matrix. *Nanomedicine* **11,** 1073–1091 (2016).
79. Bersini, S. *et al.* Human in vitro 3D co-culture model to engineer vascularized bone-mimicking tissues combining computational tools and statistical experimental approach. *Biomaterials* **76,** 157–172 (2016).
80. Arrigoni, C. *et al.* Rational Design of Prevascularized Large 3D Tissue Constructs Using Computational Simulations and Biofabrication of Geometrically Controlled Microvessels. *Adv. Healthc. Mater.* **5,** 1617–1626 (2016).
81. Middleton, K., Al-Dujaili, S., Mei, X., Günther, A. & You, L. Microfluidic co-culture platform for investigating osteocyte-osteoclast signalling during fluid shear stress mechanostimulation. *J. Biomech.* **59,** 35–42 (2017).
82. Arnaoutova, I., George, J., Kleinman, H. K. & Benton, G. The endothelial cell tube formation assay on basement membrane turns 20: State of the science and the art. *Angiogenesis* **12,** 267–274 (2009).
83. Papadimitropoulos, A. *et al.* A 3D in vitro bone organ model using human progenitor cells. *Eur. Cells Mater.* **21,** 445–458 (2011).
84. Ngo, T. X. *et al.* In Vitro Models for Angiogenesis Research : A Review. *Int. J. Tissue Regen.* **5,** 37–45 (2014).
85. Hauser, S., Jung, F. & Pietzsch, J. Human Endothelial Cell Models in Biomaterial. *Trends Biotechnol.* **35,** 265–277 (2017).
86. DeCicco-Skinner, K. L. *et al.* Endothelial Cell Tube Formation Assay for the *In Vitro* Study of Angiogenesis. *J. Vis. Exp.* **10,** 1–8 (2014).
87. Chalupowicz, D. G., Chowdhury, Z. A., Bach, T. L., Barsigian, C. & Martinez, J. Fibrin II induces endothelial cell capillary tube formation. *J Cell Biol* **130,** 207–215 (1995).
88. Montesano, R., Orci, L. & Vassalli, P. In vitro rapid organization of endothelial cells into capillary-like networks is promoted by collagen matrices. *J. Cell Biol.* **97,** 1648–1652 (1983).
89. Borra, R. C., Lotufo, M. A., Gagioti, S. M., Barros, F. de M. & Andrade, P. M. A simple method to measure cell viability in proliferation and cytotoxicity assays. *Braz. Oral Res.* **23,** 255–262 (2009).
90. Cummings, C. L., Gawlitta, D., Nerem, R. M. & Stegemann, J. P. Properties of engineered vascular constructs made from collagen, fibrin, and collagen-fibrin mixtures. *Biomaterials* **25,** 3699–3706 (2004).
91. Davis, G. E. & Senger, D. R. Endothelial extracellular matrix: Biosynthesis, remodeling, and functions during vascular morphogenesis and neovessel stabilization. *Circ. Res.* **97,** 1093–1107 (2005).
92. Rao, R. R., Peterson, A. W., Ceccarelli, J., Putnam, A. J. & Stegemann, J. P. Matrix composition regulates three-dimensional network formation by endothelial cells and mesenchymal stem cells in collagen/fibrin materials. *Angiogenesis* **15,** 253–264 (2012).
93. Critser, P. J., Kreger, S. T., Voytik-Harbin, S. L. & Yoder, M. C. Collagen matrix physical properties modulate endothelial colony forming cell-derived vessels in vivo. *Microvasc. Res.* **80,** 23–30 (2010).
94. Chung, S., Sudo, R., Zervantonakis, I. K., Rimchala, T. & Kamm, R. D. Surface-Treatment-Induced Three-Dimensional Capillary Morphogenesis in a Microfluidic Platform. *Adv. Mater.* **21,** 4863–4867 (2009).
95. Han, S. *et al.* Constructive remodeling of a synthetic endothelial extracellular matrix. *Nat. Publ. Gr.* 1–10 (2015).
96. Han, S. *et al.* Hydrophobic Patterning-Based 3D Microfluidic Cell Culture Assay. *Adv. Healthc. Mater.* **7,** 1800122 (2018).
97. Liu, J., Zheng, H., Poh, P. S. P., Machens, H. G. & Schilling, A. F. Hydrogels for engineering of perfusable vascular networks. *Int. J. Mol. Sci.* **16,** 15997–16016 (2015).
98. Wipff, P. *et al.* Biomaterials The covalent attachment of adhesion molecules to silicone membranes for cell stretching applications. *Biomaterials* **30,** 1781–1789 (2009).
99. Liu, X. D. *et al.* Endothelial cell-mediated type I collagen gel contraction is regulated

by hemin. *J. Lab. Clin. Med.* **136,** 100–9 (2000).
100. Pagella, P., Neto, E., Lamghari, M. & Mitsiadis, T. Investigation of orofacial stem cell niches and their innervation through microfluidic devices. *Eur. Cells Mater.* **29,** 213–223 (2015).
101. Nakahashi, T. *et al.* Vascular endothelial cells synthesize and secrete brain-derived neurotrophic factor. *FEBS Lett.* **470,** 113–117 (2000).
102. Yuan, Q., Li, J.-J., An, C.-H. & Sun, L. Biological characteristics of rat dorsal root ganglion cell and human vascular endothelial cell in mono- and co-culture. *Mol. Biol. Rep.* **41,** 6949–6956 (2014).
103. Yuan, Q., Sun, L., Yu, H. & An, C. Human microvascular endothelial cell promotes the development of dorsal root ganglion neurons via BDNF pathway in a co-culture system. *Biosci. Biotechnol. Biochem.* **81,** 1335–1342 (2017).
104. Stiffey-Wilusz, J., Boice, J. A., Ronan, J., Fletcher, A. M. & Anderson, M. S. An ex vivo angiogenesis assay utilizing commercial porcine carotidartery: Modification of the rat aortic ring assay. *Angiogenesis* **4,** 3–9 (2001).
105. Tan, S. H., Nguyen, N.-T., Chua, Y. C. & Kang, T. G. Oxygen plasma treatment for reducing hydrophobicity of a sealed polydimethylsiloxane microchannel. *Biomicrofluidics* **4,** 032204 (2010).
106. Kameda, T., Ishikawa, H. & Tsutsui, T. Detection and Characterization of Apoptosis in Osteoclasts in Vitro. *Biochem. Biophys. Res. Commun.* **207,** 753–760 (1995).
107. Pagani, S. *et al.* An advanced tri-culture model to evaluate the dynamic interplay among osteoblasts, osteoclasts, and endothelial cells. *J. Cell. Physiol.* **233,** 291–301 (2018).
108. Wang, Y., Wang, B., Fu, L., A, L. & Zhou, Y. Effect of Fetal Bovine Serum on Osteoclast Formation in vitro. *J. Hard Tissue Biol.* **23,** 303–308 (2014).
109. Malinda, K. M. *et al.* Identification of laminin alpha1 and beta1 chain peptides active for endothelial cell adhesion, tube formation, and aortic sprouting. *FASEB J.* **13,** 53–62 (1999).
110. Kapoor, B. R., Reddy, V. & Kapoor, P. Tube Formation Assay with Primary Human Umbilical Vein Endothelial Cells. *Lonza's Spring Resour. Notes™ Newsl.* (2013).
111. Arnaoutova, I. & Kleinman, H. K. In vitro angiogenesis: Endothelial cell tube formation on gelled basement membrane extract. *Nat. Protoc.* **5,** 628–635 (2010).